Title
Finite elastic wrinkling deformations of incompressible fiber-reinforced plates

Authors
Taylor, M
Shirani, M
Dabiri, Y
et al.

Publication Date
2019-11-01

DOI
10.1016/j.ijengsci.2019.103138

Peer reviewed

HHS Public Access

Author manuscript

Int J Eng Sci. Author manuscript; available in PMC 2020 November 01.

Published in final edited form as:

Int J Eng Sci. 2019 November ; 144: . doi:10.1016/j.ijengsci.2019.103138.

Finite elastic wrinkling deformations of incompressible fiber-reinforced plates

M. Taylor[a,*], **M. Shirani**[b], **Y. Dabiri**[c], **J. M. Guccione**[c], **D. J. Steigmann**[b]

[a]Department of Mechanical Engineering, Santa Clara University, Santa Clara, CA 95053 USA

[b]Department of Mechanical Engineering, University of California, Berkeley, CA 94720 USA

[c]Department of Surgery, University of California, San Francisco, CA 94143 USA

Abstract

A two-dimensional plate theory, valid for finite elastic deformations with small strains, is derived for incompressible, fiber-reinforced materials. Single-layer plates and two-layer laminates are considered. Numerical simulations illustrate the substantial effect that fiber reinforcement has on wrinkling patterns in the sheet.

Keywords

Nonlinear plate theory; anisotropy; wrinkling; dynamic relaxation

1. Introduction

The nonlinear elastic response of thin sheets is of great significance in technology and biology. For example, the mitral valve of the heart may be viewed as a thin bio-elastic sheet with fairly complex mechanical properties conferred by a fibrous, laminated substructure in which each lamina is reinforced by one or two families of fibers (Wenk et al., 2012; Zhang et al., 2016). This structure is the subject of considerable current research (Grashow et al., 2006a,b; Ayoub et al., 2016; Sacks and Yoganathan, 2007), which, however, is typically based on modeling that appears to us to be somewhat *ad hoc* by the standards of the Mechanics community. This circumstance furnishes impetus for the present work, concerned with the careful development of a two-dimensional framework for thin, fiber-reinforced, incompressible elastic sheets.

*Corresponding author: mjtaylor@scu.edu (M. Taylor).

Conflict of Interest Statement

The authors certify that they have NO affiliations with or involvement in any organization or entity with any financial interest (such as honoraria; educational grants; participation in speakers bureaus; membership, employment, consultancies, stock ownership, or other equity interest; and expert testimony or patent-licensing arrangements), or non-financial interest (such as personal or professional relationships, affiliations, knowledge or beliefs) in the subject matter or materials discussed in this manuscript. Declarations of interest: none

We begin in Section 2 with a review of the constitutive structure of three-dimensional elasticity for incompressible materials and its specialization to the small-strain, finite-deformation regime where contact is made with Spencer's formulation (Spencer, 1984) for transversely isotropic and orthotropic materials. These model materials are reinforced, respectively, by either one family of fibers or by two families of initially orthogonal fibers. A two-dimensional strain energy is then derived in Section 3, for both single laminae and for two-ply laminates, by an asymptotic analysis of the three-dimensional energy for a thin sheet. This is used in Section 4 to derive the equilibrium theory for thin plates on the basis of a virtual-power postulate. The formal similarity of the present theory to the theory of second-grade elasticity is emphasized to aid in its interpretation. In Section 5, we outline a computational procedure, used in a related work (Taylor et al., 2014) concerned with the wrinkling of isotropic plates, for solving the relevant equilibrium equations. For the sake of brevity and to avoid duplication, we confine ourselves to a description of this method and refer the interested reader to that work for a full exposition. Finally, in Section 6 we discuss a number of examples intended to highlight the effects of fiber reinforcement. These illustrate the substantial effect of anisotropy on wrinkling patterns in thin sheets. Indeed, plate wrinkling is currently an active field of research, albeit typically limited to isotropic materials, e.g., (Puntel et al., 2011; Nayyar et al., 2011; Healey et al., 2013; Taylor et al., 2014; Qin et al., 2014; Taylor et al., 2015; Fu et al., 2019; Wang et al., 2019), with notable exceptions including studies of orthotropic sheets using finite elements (Woo et al., 2004; Gerngross and Pellegrino, 2009; Deng and Pellegrino, 2012) and an extended finite Föppl-von Kármán model (Sipos and Fehér, 2016). Our main objective in the present work is to expand the scope of this field to encompass certain types of anisotropy in a framework derived from three-dimensional elasticity.

Standard notation is adopted throughout. Thus, we use bold face for vectors and tensors and indices to denote their Cartesian components. Latin indices take values in {1,2,3}; Greek in {1,2}. The latter are associated with surface coordinates and associated vector and tensor components, and the usual summation convention for repeated subscripts is adopted. The notation $\otimes$ identifies the standard tensor product of vectors and a dot between bold symbols is used to denote the Euclidean inner product. Thus, if $\mathbf{A}_1$ and $\mathbf{A}_2$ are second-order tensors, then $\mathbf{A}_1 \cdot \mathbf{A}_2 = tr(\mathbf{A}_1\mathbf{A}_2^t)$, where $tr(\cdot)$ is the trace and the superscript ^{t} is used to denote the transpose. The norm of a tensor $\mathbf{A}$ is $|\mathbf{A}| = \sqrt{\mathbf{A}\cdot\mathbf{A}}$ and its determinant is det $\mathbf{A}$. Its inverse $\mathbf{A}^{-1}$ exists and is unique if and only if det $\mathbf{A} \neq 0$. The notation $Sym\mathbf{A}$, $Dev\mathbf{A}$ and $Sph\mathbf{A}$ is used to denote the symmetric, deviatoric and spherical parts of $\mathbf{A}$, respectively, whereas *Sym, Dev* and *Sph* are the linear spaces of symmetric, deviatoric and spherical tensors. If $\mathscr{M}$ is a fourth-order tensor, then $\mathscr{M}[\mathbf{A}]$ is the second-order tensor with Cartesian components $\mathscr{M}_{iAjB}A_{jB}$. We use *Div* to denote the three-dimensional divergence operator, and *div* to denote its two-dimensional counterpart. For example, $Div\mathbf{A} = A_{iA,A}\mathbf{e}_i$ and $div\mathbf{A} = A_{i\alpha,\alpha}\mathbf{e}_i$, where $\{\mathbf{e}_i\}$ is an orthonormal basis in which subscripts preceded by commas are used to denote partial derivatives with respect to Cartesian coordinates, and the unit vector $\mathbf{k} = \mathbf{e}_3$ identifies the orientation of the plate midplane prior to deformation. We also use ∇ to denote the two-dimensional gradient on this plane. Finally, $F_{\mathbf{A}}$ stands for the tensor-valued derivative of a scalar-valued function $F(\mathbf{A})$ with respect to its tensor argument.

2. Three-dimensional constitutive theory

We consider hyperelastic materials endowed with strain-energy functions of the form $W(\mathbf{F}; \mathbf{x})$, where $\mathbf{x}$ is the position of a material point in a reference configuration κ of the body and $\mathbf{F}$ is the gradient of the deformation $\chi(\mathbf{x})$. Here, the explicit dependence of W on $\mathbf{x}$ accommodates a possible non-uniformity of the material due, for example, to a spatial distribution of reinforcing fibers.

The 1st Piola-Kirchhoff stress $\mathbf{P}$ is given by

$$\mathbf{P} = W_{\mathbf{F}} - p\mathbf{F}^*, \tag{1}$$

where $\mathbf{F}^* = J\mathbf{F}^{-t}$ is the cofactor of $\mathbf{F}$, $J = \det \mathbf{F}$ and p is a Lagrange multiplier associated with the constraint of incompressibility ($J = 1$). Here, for the purpose of calculating the derivative $W_{\mathbf{F}}$, W is regarded as a smooth extension of the strain-energy function from the constraint manifold defined by $J = 1$ to the set defined by $\det \mathbf{F} > 0$; the derivative is then evaluated on the manifold. It is well known that the strain-energy function is frame-invariant if and only if it depends on $\mathbf{F}$ through the Cauchy-Green deformation tensor $\mathbf{C} = \mathbf{F}^t\mathbf{F}$ or, equivalently, through the Lagrange strain $\mathbf{E} = \frac{1}{2}(\mathbf{C} - \mathbf{I})$, where $\mathbf{I}$ is the identify for 3-space; we write $W(\mathbf{F}; \mathbf{x}) = U(\mathbf{E}; \mathbf{x})$. This furnishes the 2nd Piola-Kirchhoff stress $\mathbf{S}$, related to $\mathbf{P}$ by

$$\mathbf{P} = \mathbf{F}\mathbf{S}. \tag{2}$$

Thus,

$$\mathbf{S} = U_{\mathbf{E}} - p\mathbf{C}^{-1}, \tag{3}$$

where, again, U is a smooth extension from the manifold defined by $\det(\mathbf{I} + 2\mathbf{E}) = 1$ and the derivative is evaluated, post facto, on the manifold.

It is well known (Steigmann, 2017) that the difference of the derivatives of two extensions of the energy is orthogonal to the local tangent space to the constraint manifold and may therefore be absorbed into the Lagrange multiplier. Thus any one extension may be used without loss of generality.

Consider a one-parameter family $\chi(\mathbf{x}; \epsilon)$ of deformations. This induces the one-parameter families $\mathbf{F}(\mathbf{x}; \epsilon)$ and $\mathbf{E}(\mathbf{x}; \epsilon)$. We differentiate the equation $W = U$ with respect to the parameter, on the constraint manifold, obtaining

$$W_{\mathbf{F}} \cdot \dot{\mathbf{F}} = U_{\mathbf{E}} \cdot \dot{\mathbf{E}}, \quad \text{with} \quad \dot{\mathbf{E}} = Sym(\mathbf{F}^t\dot{\mathbf{F}}), \tag{4}$$

or, equivalently,

$$W_{\mathbf{F}} \cdot \dot{\mathbf{F}} = \mathbf{F}(U_{\mathbf{E}}) \cdot \dot{\mathbf{F}}, \tag{5}$$

in which $\dot{\mathbf{F}}$ is restricted by the requirement $\dot{J} = 0$. With $J_{\mathbf{F}} = \mathbf{F}^*$ the latter implies that

$$\mathbf{F}^{*} \cdot \dot{\mathbf{F}} = 0 \tag{6}$$

and $\dot{\mathbf{F}}$ is otherwise arbitrary.

A further differentiation yields

$$W_{\mathbf{FF}}[\dot{\mathbf{F}}] \cdot \dot{\mathbf{F}} + W_{\mathbf{F}} \cdot \ddot{\mathbf{F}} = U_{\mathbf{EE}}[\dot{\mathbf{E}}] \cdot \dot{\mathbf{E}} + U_{\mathbf{E}} \cdot \ddot{\mathbf{E}}, \quad \text{with} \quad \ddot{\mathbf{E}} = \dot{\mathbf{F}}^{t}\dot{\mathbf{F}} + Sym(\mathbf{F}^{t}\ddot{\mathbf{F}}), \tag{7}$$

or, equivalently,

$$W_{\mathbf{FF}}[\dot{\mathbf{F}}] \cdot \dot{\mathbf{F}} + W_{\mathbf{F}} \cdot \ddot{\mathbf{F}} = \mathbf{F}^{t}\dot{\mathbf{F}} \cdot U_{\mathbf{EE}}[\mathbf{F}^{t}\dot{\mathbf{F}}] + \mathbf{F}(U_{\mathbf{E}}) \cdot \ddot{\mathbf{F}} + U_{\mathbf{E}} \cdot \dot{\mathbf{F}}^{t}\dot{\mathbf{F}}, \tag{8}$$

in which the minor symmetries of $U_{\mathbf{EE}}$ have been used, all derivatives are evaluated on the constraint manifold, and $\ddot{\mathbf{F}}$ is restricted by the requirement $\ddot{J} = 0$, i.e.

$$\mathbf{F}^{*} \cdot \ddot{\mathbf{F}} + \mathbf{F}^{*}_{\mathbf{F}}[\dot{\mathbf{F}}] \cdot \dot{\mathbf{F}} = 0. \tag{9}$$

The 4th-order tensor $\mathbf{F}^{*}_{\mathbf{F}}$ is given, in terms of the Cartesian components F_{iA} of $\mathbf{F}$, by (Steigmann, 2017)

$$J\,\partial F^{*}_{iA} / \partial F_{jB} = F^{*}_{iA}F^{*}_{jB} - F^{*}_{jA}F^{*}_{iB}\,. \tag{10}$$

With $J = 1$, this furnishes

$$\mathbf{F}^{*}_{\mathbf{F}}[\dot{\mathbf{F}}] = (\mathbf{F}^{*} \cdot \dot{\mathbf{F}})\mathbf{F}^{*} - F^{*}_{iB}F^{*}_{jA}\dot{F}_{jB}, \tag{11}$$

which combines with (6) and (9) to give

$$\mathbf{F}^{*} \cdot \ddot{\mathbf{F}} = F^{*}_{iB}F^{*}_{jA}\dot{F}_{jB}\dot{F}_{iA}, \tag{12}$$

whereas the part of $\ddot{\mathbf{F}}$ orthogonal to $\mathbf{F}^{*}$ is arbitrary.

Consider the rank-one form $\dot{\mathbf{F}} = \mathbf{p} \otimes \mathbf{q}$. This yields $\mathbf{F}^{*} \cdot \ddot{\mathbf{F}} = (\mathbf{p} \cdot \mathbf{F}^{*}\mathbf{q})^{2}$, which vanishes because

$$\mathbf{p} \cdot \mathbf{F}^{*}\mathbf{q} = 0 \tag{13}$$

in accordance with (6). Because of (5) and (6), we then have

$$W_{\mathbf{F}} \cdot \ddot{\mathbf{F}} = \mathbf{F}(U_{\mathbf{E}}) \cdot \ddot{\mathbf{F}} \tag{14}$$

and (8) reduces to

$$W_{\mathbf{FF}}[\mathbf{p} \otimes \mathbf{q}] \cdot \mathbf{p} \otimes \mathbf{q} = \mathbf{F}^{t}\mathbf{p} \otimes \mathbf{q} \cdot U_{\mathbf{EE}}[\mathbf{F}^{t}\mathbf{p} \otimes \mathbf{q}] + |\mathbf{p}|^{2}\mathbf{q} \cdot (U_{\mathbf{E}})\mathbf{q}\,. \tag{15}$$

The strong-ellipticity condition is

$$W_{\mathbf{FF}}[\mathbf{p}\otimes\mathbf{q}]\cdot\mathbf{p}\otimes\mathbf{q}>0 \tag{16}$$

for all $\mathbf{p}\otimes\mathbf{q}\neq\mathbf{0}$ subject to (13) (Fosdick and MacSithigh, 1986). Accordingly, if the deformation is such that the strong-ellipticity condition is satisfied, then the right-hand side of (15) is positive with the same proviso. Supposing strong ellipticity to be satisfied at the undeformed state $\mathbf{F}=\mathbf{I}$, and that $U_{\mathbf{E}}$ vanishes at $\mathbf{E}=\mathbf{0}$, we then have

$$\mathbf{p}\otimes\mathbf{q}\cdot\mathscr{C}[\mathbf{p}\otimes\mathbf{q}]>0 \tag{17}$$

for all $\mathbf{p}\otimes\mathbf{q}\neq\mathbf{0}$ subject to $\mathbf{p}\cdot\mathbf{q}=0$, where $\mathscr{C}=U_{\mathbf{EE}}(\mathbf{0})$ is the classical elasticity tensor. This makes sense because $\mathbf{p}\otimes\mathbf{q}$ vanishes if and only if $Sym(\mathbf{p}\otimes\mathbf{q})$ vanishes. Conventionally, (17) is ensured by requiring that $\mathscr{C}$ be positive definite in the sense that

$$\mathbf{A}\cdot\mathscr{C}[\mathbf{A}]>0 \tag{18}$$

for all non-zero symmetric $\mathbf{A}$ with $tr\mathbf{A}=0$. This in turn follows from the inequality $\ddot{U}>0$, evaluated at $\mathbf{F}=\mathbf{I}$, with $U_{\mathbf{E}}=\mathbf{0}$ at $\mathbf{E}=\mathbf{0}$ and with $Sym\dot{\mathbf{F}}=\mathbf{A}$ restricted in accordance with (6), i.e. $\mathbf{I}\cdot\mathbf{A}=0$.

For small strains of incompressible materials, it is well known that $\mathbf{E}$ is deviatoric at leading order. This follows by expanding $J^2=\det(\mathbf{I}+2\mathbf{E})$ with $J=1$, yielding

$$tr\mathbf{E}=|\mathbf{E}|^2-(tr\mathbf{E})^2-4\det\mathbf{E}, \tag{19}$$

which implies that $\mathbf{E}=Dev\mathbf{E}+Sph\mathbf{E}$ with $|Sph\mathbf{E}|=O(|\mathbf{E}|^2)$. The leading-order small-strain approximation to the strain energy is then given by

$$U(\mathbf{E})=Q(Dev\mathbf{E})+o(|\mathbf{E}|^2), \tag{20}$$

with

$$Q(\mathbf{E})=\frac{1}{2}\mathbf{E}\cdot\mathscr{C}[\mathbf{E}]\,. \tag{21}$$

The latter expression furnishes the obvious extension of the leading-order energy $Q(Dev\mathbf{E})$ for use in computing the derivative $U_{\mathbf{E}}$.

In the present work we consider materials reinforced by a single family of fibers and by two families of initially orthogonal fibers with distinct mechanical properties. The first of these types is transversely isotropic, with (Spencer, 1984)

$$\mathscr{C}[\mathbf{E}]=2\mu_T\mathbf{E}+2(\mu_L-\mu_T)(\mathbf{E}\mathbf{a}\otimes\mathbf{a}+\mathbf{a}\otimes\mathbf{E}\mathbf{a})+\beta(\mathbf{a}\cdot\mathbf{E}\mathbf{a})\mathbf{a}\otimes\mathbf{a}, \tag{22}$$

where $\mathbf{a}$ is the unit-tangent field to the fiber trajectories in κ. The moduli μ_T and μ_L respectively are the shear moduli for shearing in planes transverse and parallel to the fibers,

and β contributes to the extensional stiffness along the fibers. The second type of material is orthotropic, with (Spencer, 1984)

$$\begin{aligned}\mathscr{C}[\mathbf{E}] &= 2\mu\mathbf{E} + 2\mu_a(\mathbf{E}\mathbf{a}\otimes\mathbf{a} + \mathbf{a}\otimes\mathbf{E}\mathbf{a}) + 2\mu_b(\mathbf{E}\mathbf{b}\otimes\mathbf{b} + \mathbf{b}\otimes\mathbf{E}\mathbf{b})\\ &+ (\beta_a\mathbf{a}\cdot\mathbf{E}\mathbf{a} + \beta_{ab}\mathbf{b}\cdot\mathbf{E}\mathbf{b})\mathbf{a}\otimes\mathbf{a} + (\beta_{ab}\mathbf{a}\cdot\mathbf{E}\mathbf{a} + \beta_b\mathbf{b}\cdot\mathbf{E}\mathbf{b})\mathbf{b}\otimes\mathbf{b},\end{aligned} \tag{23}$$

where $\mathbf{a}$ and $\mathbf{b}$, with $\mathbf{a}\cdot\mathbf{b} = 0$, are the unit-tangent fields to the two fiber families. Here μ, μ_a and μ_b are shear moduli, and we refer to Spencer (1984) for interpretations of these and of β_a, β_b and β_{ab} in terms of the conventional engineering moduli.

We have

$$U_{\mathbf{E}} = \mathscr{C}[\mathbf{E}] + o(|\mathbf{E}|), \tag{24}$$

and with $\mathbf{C}^{-1} = \mathbf{I} + O(|\mathbf{E}|)$, the leading-order approximation to the stress $\mathbf{S}$ is

$$\mathbf{S} \simeq \mathscr{C}[Dev\mathbf{E}] - p\mathbf{I}, \tag{25}$$

in which we have evaluated the derivative $U_{\mathbf{E}}$ on the constraint manifold, as required by (3). The latter is approximated at leading order by its tangent space at $\mathbf{E} = \mathbf{0}$, i.e. by the linear space *Dev*. Of course the spherical part of $\mathscr{C}[Dev\mathbf{E}]$ may be absorbed into the multiplier p, but it is quite unnecessary to do so. The expression (25) for the stress coincides precisely with that given in Spencer (1984).

In this work we take the fibers to lie parallel to a fixed plane with unit normal $\mathbf{k}$, so that $\mathbf{a}\cdot\mathbf{k} = 0$ and $\mathbf{b}\cdot\mathbf{k} = 0$. With $\mathbf{A} = Sym(\mathbf{p}\otimes\mathbf{q})$ and $\mathbf{p}\cdot\mathbf{q} = 0$, the strong-ellipticity condition (17) for transversely isotropic materials becomes

$$0 < \mu_T|\mathbf{p}|^2|\mathbf{q}|^2 + (\mu_L - \mu_T)[|\mathbf{p}|^2(\mathbf{q}\cdot\mathbf{a})^2 + |\mathbf{q}|^2(\mathbf{p}\cdot\mathbf{a})^2] + \frac{1}{2}\beta(\mathbf{p}\cdot\mathbf{a})^2(\mathbf{q}\cdot\mathbf{a})^2\cdot \tag{26}$$

To derive necessary conditions, we choose $\mathbf{q} = \mathbf{k}$ with $\mathbf{p} = p_a\mathbf{a} + p_b\mathbf{b}$, obtaining

$$\mu_L p_a^2 + \mu_T p_b^2 > 0 \tag{27}$$

for all p_a, p_b with $p_a^2 + p_b^2 > 0$; thus,

$$\mu_L > 0 \quad \text{and} \quad \mu_T > 0. \tag{28}$$

In the case of orthotropy, after some calculation we find that (17) becomes

$$\begin{aligned}0 \quad < \quad & \mu|\mathbf{p}|^2|\mathbf{q}|^2 + \mu_a[|\mathbf{p}|^2(\mathbf{q}\cdot\mathbf{a})^2 + |\mathbf{q}|^2(\mathbf{p}\cdot\mathbf{a})^2] + \mu_b[|\mathbf{p}|^2(\mathbf{q}\cdot\mathbf{b})^2 + |\mathbf{q}|^2(\mathbf{p}\cdot\mathbf{b})^2]\\ &+ \frac{1}{2}\beta_a(\mathbf{p}\cdot\mathbf{a})^2(\mathbf{q}\cdot\mathbf{a})^2 + \frac{1}{2}\beta_b(\mathbf{p}\cdot\mathbf{b})^2(\mathbf{q}\cdot\mathbf{b})^2 + \beta_{ab}(\mathbf{p}\cdot\mathbf{a})(\mathbf{q}\cdot\mathbf{a})(\mathbf{p}\cdot\mathbf{b})(\mathbf{q}\cdot\mathbf{b})\,.\end{aligned} \tag{29}$$

Choosing $\mathbf{q}$ and $\mathbf{p}$ as before, we derive

$$(\mu + \mu_a)p_a^2 + (\mu + \mu_b)p_b^2 > 0 \tag{30}$$

and conclude that

$$\mu + \mu_a > 0 \quad \text{and} \quad \mu + \mu_b > 0. \tag{31}$$

Of course the necessary conditions (28) and (31) are not sufficient for strong ellipticity, but they do suffice for our purposes. Detailed discussions of strong ellipticity for transversely isotropic and orthotropic materials are given in Payton (1983); Merodio and Ogden (2003) and Aguiar (2019), respectively. We discuss inequality (18) for the two material types in Section 3.2.

3. Asymptotic derivation of the leading-order plate energy for combined bending and stretching

3.1. Descent from three dimensions to two

Position in the reference placement of the plate may be written

$$\mathbf{x} = \mathbf{u} + \varsigma\mathbf{k}, \tag{32}$$

where $\mathbf{u} \in \Omega$, Ω is the midplane of the plate, $\varsigma \in [-h/2, h/2]$ is a through-thickness coordinate and h is the plate thickness, assumed to be much smaller than the next smallest length scale, l say, in a given problem. We simplify the notation by adopting l as the unit of length ($l = 1$); then, the dimensionless thickness $h << 1$.

The strain energy associated with a given deformation is

$$\mathscr{E} = \int_\kappa U(\widetilde{\mathbf{E}}(\mathbf{x}))dv = \int_\Omega \int_{-h/2}^{h/2} U(\widetilde{\mathbf{E}}(\mathbf{u} + \varsigma\mathbf{k}))d\varsigma da, \tag{33}$$

where $\widetilde{\mathbf{E}}(\mathbf{x})$ is the three-dimensional strain. If this is sufficiently smooth, then by Leibniz' Rule and Taylor's Theorem, applied to h (Shirani and Steigmann, 2019), we find that the areal energy density on Ω is given, for small h, by

$$\int_{-h/2}^{h/2} U(\widetilde{\mathbf{E}}(\mathbf{u} + \varsigma\mathbf{k}))d\varsigma = hU + \frac{1}{24}h^3U'' + o(h^3), \tag{34}$$

where primes are used to denote derivatives with respect to ς, $\mathbf{E}(\mathbf{u}) = \widetilde{\mathbf{E}}_{|\Omega}$ is the midplane strain, U is evaluated at $\mathbf{E}(\mathbf{u})$ and, by the chain rule,

$$U' = U_{\mathbf{E}} \cdot \mathbf{E}' \quad \text{and} \quad U'' = U_{\mathbf{EE}}[\mathbf{E}'] \cdot \mathbf{E}' + U_{\mathbf{E}} \cdot \mathbf{E}'' \tag{35}$$

in which the derivatives $U_{\mathbf{E}}$ and $U_{\mathbf{EE}}$ are evaluated at $\mathbf{E}(\mathbf{u})$, and

$$\mathbf{E}^{(n)} = \widetilde{\mathbf{E}}^{(n)}_{|\varsigma=0}. \tag{36}$$

Here, we assume that there is no variation of material properties in the direction orthogonal to Ω, so that U depends on ς only implicitly, via $\widetilde{\mathbf{E}}(\mathbf{x})$. The material moduli, the thickness h, and the fiber directions **a** and **b** may, however, depend on $\mathbf{u} \in \Omega$.

If $\widetilde{\mathbf{F}}(\mathbf{x})$ is the gradient of the three-dimensional deformation $\widetilde{\chi}(\mathbf{x})$, then

$$\widetilde{\mathbf{F}} = \nabla\widetilde{\chi} + \widetilde{\chi}' \otimes \mathbf{k}, \tag{37}$$

where ∇ is the (two-dimensional) gradient with respect to **u** on Ω. Its first and second derivatives with respect to ς are

$$\widetilde{\mathbf{F}}' = \nabla\widetilde{\chi}' + \widetilde{\chi}'' \otimes \mathbf{k} \quad \text{and} \quad \widetilde{\mathbf{F}}'' = \nabla\widetilde{\chi}'' + \widetilde{\chi}''' \otimes \mathbf{k}, \tag{38}$$

and these reduce, on the midplane, to

$$\mathbf{F} = \nabla\mathbf{r} + \mathbf{d} \otimes \mathbf{k}, \quad \mathbf{F}' = \nabla\mathbf{d} + \mathbf{g} \otimes \mathbf{k}, \quad \text{and} \quad \mathbf{F}'' = \nabla\mathbf{g} + \mathbf{h} \otimes \mathbf{k}, \tag{39}$$

where

$$\mathbf{r}(\mathbf{u}) = \widetilde{\chi}_{|\Omega} \tag{40}$$

is the midplane deformation, and

$$\mathbf{d}(\mathbf{u}) = \widetilde{\chi}'_{|\,\Omega}, \quad \mathbf{g}(\mathbf{u}) = \widetilde{\chi}''_{|\,\Omega} \quad \text{and} \quad \mathbf{h}(\mathbf{u}) = \widetilde{\chi}'''_{|\,\Omega}. \tag{41}$$

are *independent* functions of **u**. These are the coefficient vectors in the order - ς^3 expansion

$$\widetilde{\chi}(\mathbf{u} + \varsigma\mathbf{k}) = \mathbf{r}(\mathbf{u}) + \varsigma\mathbf{d}(\mathbf{u}) + \frac{1}{2}\varsigma^2\mathbf{g}(\mathbf{u}) + \frac{1}{6}\varsigma^3\mathbf{h}(\mathbf{u}) + \dots. \tag{42}$$

Here, **r**(**u**) is the position of a material point on the deformed image ω of the midplane Ω; its gradient $\nabla\mathbf{r}$ maps the translation space Ω' of Ω to the tangent plane T_ω to the surface ω at the material point **u**. The functions **d**(**u**), **g**(**u**) and **h**(**u**) provide information about the three-dimensional deformation in the vicinity of the midplane.

Further, in (34) and (35) we have (compare $(4)_2$, $(7)_2$)

$$\mathbf{E} = \frac{1}{2}(\mathbf{F}^t\mathbf{F} - \mathbf{I}), \quad \mathbf{E}' = Sym(\mathbf{F}^t\mathbf{F}') \quad \text{and} \quad \mathbf{E}'' = (\mathbf{F}')^t\mathbf{F}' + Sym(\mathbf{F}^t\mathbf{F}''), \tag{43}$$

in which **F**, $\mathbf{F}'$ and $\mathbf{F}''$ are restricted by bulk incompressibility, i.e. by the constraints $J = 1$, $J' = J'' = 0$. In particular, we may use $J = \mathbf{Fk} \cdot \mathbf{F}^*\mathbf{k}$ with the Piola-Nanson formula $\mathbf{F}^*\mathbf{k} = a\mathbf{n}$, where **n** is the unit normal to T_ω and $a = |\mathbf{F}^*\mathbf{k}|$ is the areal stretch of Ω, together with $J = 1$ and $(39)_1$, to conclude that (Steigmann, 2017)

$$\mathbf{d} = \alpha^{-1}\mathbf{n} + (\nabla \mathbf{r})\mathbf{e}, \tag{44}$$

for some 2-vector $\mathbf{e} \in \Omega'$. Here we note that $\mathbf{F}^*\mathbf{k} = \mathbf{F}\mathbf{e}_1 \times \mathbf{F}\mathbf{e}_2 = (\nabla \mathbf{r})\mathbf{e}_1 \times (\nabla \mathbf{r})\mathbf{e}_2$, where $\{\mathbf{e}_\alpha\}$ is any orthonormal basis for Ω' such that $\mathbf{e}_1 \times \mathbf{e}_2 \cdot \mathbf{k} = 1$. Thus, $\mathbf{d}$ is determined by $\nabla \mathbf{r}$ and $\mathbf{e}$.

In the same way, we use $0 = J' = \mathbf{F}^* \cdot \mathbf{F}'$ with $(39)_2$, concluding that $\mathbf{g} \cdot \mathbf{n} = -\alpha^{-1}\mathbf{F}^* \cdot \nabla \mathbf{d}$ and hence that

$$\mathbf{g} = (\nabla \mathbf{r})\mathbf{f} - \alpha^{-1}(\mathbf{F}^* \cdot \nabla \mathbf{d})\mathbf{n} \tag{45}$$

for some 2-vector $\mathbf{f} \in \Omega'$. A similar procedure may be used to derive a representation for $\mathbf{h}$, etc., if desired.

Corresponding to (44), the Cauchy-Green deformation tensor $\mathbf{C} = \mathbf{F}^t\mathbf{F}$ is

$$\mathbf{C} = \mathbf{c} + \mathbf{c}\mathbf{e} \otimes \mathbf{k} + \mathbf{k} \otimes \mathbf{c}\mathbf{e} + (\alpha^{-2} + \mathbf{e} \cdot \mathbf{c}\mathbf{e})\mathbf{k} \otimes \mathbf{k}, \quad \text{where} \quad \mathbf{c} = (\nabla \mathbf{r})^t(\nabla \mathbf{r}) \tag{46}$$

is the *surfacial* Cauchy-Green deformation tensor; this has the property

$$\det \mathbf{c} = \alpha^2 . \tag{47}$$

The associated strain is

$$\mathbf{E} = \varepsilon + Sym(\gamma \otimes \mathbf{k}) + \bar{E}\mathbf{k} \otimes \mathbf{k}, \tag{48}$$

where

$$\gamma = \mathbf{c}\mathbf{e}, \quad \bar{E} = \frac{1}{2}(\alpha^{-2} - 1 + \mathbf{e} \cdot \mathbf{c}\mathbf{e}) \quad \text{and} \quad \varepsilon = \frac{1}{2}(\mathbf{c} - \mathbf{1}) \tag{49}$$

is the surface strain, in which

$$\mathbf{1} = \mathbf{I} - \mathbf{k} \otimes \mathbf{k} \tag{50}$$

is the projection onto Ω' and γ is evidently the transverse shear strain. Accordingly, for small $|\mathbf{E}|$, incompressibility yields $\bar{E} = -tr\varepsilon + O(|\mathbf{E}|^2)$, so that $Dev\mathbf{E} = \bar{\mathbf{E}} + O(|\mathbf{E}|^2)$, with

$$\bar{\mathbf{E}} = \varepsilon - (tr\varepsilon)\mathbf{k} \otimes \mathbf{k} + Sym(\gamma \otimes \mathbf{k}) . \tag{51}$$

We are interested in applications involving finite deformations with small-to-moderate midplane strains. This suffices for most engineering applications (Koiter, 1960, 1966; Ciarlet, 2005). Further applications of contemporary interest in biomechanics include mitral heart valves, which typically experience principal stretches that are close to unity (Grashow et al., 2006a,b). In such circumstances, it is appropriate to adopt an estimate of the energy (34) in which the separate order - h and order - h^3 terms are replaced by their leading-order approximations for small $|\mathbf{E}|$. For example, in (34) we have

$$U = Q(\bar{\mathbf{E}}) + o(|\mathbf{E}|^2), \tag{52}$$

where $\bar{\mathbf{E}}$ is given by (51). Similarly, from (24) we have $U_{\mathbf{E}} = \mathscr{C}[\mathbf{E}] + o(|\mathbf{E}|) = O(|\mathbf{E}|)$, whereas $U_{\mathbf{EE}} = \mathscr{C} + O(|\mathbf{E}|)$. From $(35)_2$ we then have $U'' = \mathbf{E}' \cdot \mathscr{C}[\mathbf{E}'] + O(|\mathbf{E}|)$, in which $\mathbf{E}'$ - given by $(43)_2$ - is estimated by observing that the right-stretch factor $\mathbf{U}$ in the polar decomposition $\mathbf{F} = \mathbf{RU}$ of the deformation gradient, in which $\mathbf{R}$ is a rotation, satisfies $\mathbf{U} = \mathbf{I} + O(|\mathbf{E}|)$. Then,

$$\mathbf{E}' = Sym(\mathbf{R}^t\mathbf{F}') + O(|\mathbf{E}|), \tag{53}$$

yielding

$$U'' = \mathbf{R}^t\mathbf{F}' \cdot \mathscr{C}[\mathbf{R}^t\mathbf{F}'] + O(|\mathbf{E}|)\,. \tag{54}$$

Combining this with (33) and (34), we obtain

$$\mathscr{E} = E + o(h^3), \tag{55}$$

where

$$E = \int_\Omega W\, da, \tag{56}$$

with

$$W \simeq hQ(\bar{\mathbf{E}}) + \frac{1}{12}h^3 Q(\mathbf{R}^t\mathbf{F}'), \tag{57}$$

in which both terms are valid to leading order in $|\mathbf{E}|$.

Note that $tt(\mathbf{R}^t\mathbf{F}') = \mathbf{R} \cdot \mathbf{F}' = \mathbf{R}^* \cdot \mathbf{F}'$, where $\mathbf{R}^*$ is the cofactor of $\mathbf{R}$; this coincides with $\mathbf{R}$ because $\mathbf{R}$ is a rotation. Then, because $\mathbf{F}^* = \mathbf{R}^*\mathbf{U}^*$, and with $\mathbf{U}^* = \mathbf{I} + O(|\mathbf{E}|)$, we have $\mathbf{R}^* = \mathbf{F}^* + O(|\mathbf{E}|)$, yielding $tt(\mathbf{R}^t\mathbf{F}') = O(|\mathbf{E}|)$ on account of $\mathbf{F}^* \cdot \mathbf{F}' (= J') = 0$. Thus $\mathbf{R}^t\mathbf{F}'$ is deviatoric at leading order, i.e. at order unity. Because $\bar{\mathbf{E}}$ is also deviatoric, this means that the plate energy W is fully specified by (21), in which $\mathscr{C}[Dev\mathbf{E}]$ is given by (22) or (23) as appropriate.

The energy W involves the vector fields $\mathbf{d}$ and $\mathbf{g}$ via $(39)_{1,2}$. These in turn involve the 2-vectors $\mathbf{e}$ and $\mathbf{f}$, which at this stage are kinematically independent of the midplane deformation $\mathbf{r}$. This suggests a strategy whereby we attempt to render the energy stationary with respect to these fields *a priori*. For example, E is stationary with respect to $\mathbf{e}$ at fixed $\nabla\mathbf{r}$ and $\mathbf{f}$ if and only if

$$hQ_{\mathbf{E}}(\bar{\mathbf{E}}) \cdot (\bar{\mathbf{E}})^{\cdot} + O(h^3) = 0, \tag{58}$$

where the superposed dot refers to a variational derivative, and (cf. (51))

$$(\overline{\mathbf{E}})^{\cdot} = Sym(\dot{\gamma} \otimes \mathbf{k}), \quad \text{with} \quad \dot{\gamma} = \mathbf{c}\dot{\mathbf{e}}\,. \tag{59}$$

Dividing (58) by h and passing to the limit, we obtain

$$\dot{\gamma} \cdot (\mathscr{C}[\overline{\mathbf{E}}])\mathbf{k} = 0 \tag{60}$$

at leading order, in which $\dot{\gamma} \in \Omega'$ is arbitrary. Thus,

$$\mathbf{1}(\mathscr{C}[\overline{\mathbf{E}}])\mathbf{k} = \mathbf{0}, \tag{61}$$

where $\mathbf{1}$ is the projection onto Ω'.

For transversely isotropic materials, (22) is used to reduce this to

$$\mu_T \gamma + (\mu_L - \mu_T)(\mathbf{a} \cdot \gamma)\mathbf{a} = \mathbf{0}\,. \tag{62}$$

Decomposing γ in the basis $\{\mathbf{a}, \mathbf{b}\}$, with $\mathbf{b} = \mathbf{k} \times \mathbf{a}$, and invoking the strong-ellipticity inequalities (28), we conclude that $\gamma = \mathbf{0}$. Moreover, a further consequence of strong-ellipticity is that this solution is energetically optimal (Steigmann, 2017; Shirani and Steigmann, 2019).

For orthotropic materials, (23) is used to reduce (61) to

$$(\mu + \mu_a)(\mathbf{a} \cdot \gamma)\mathbf{a} + (\mu + \mu_b)(\mathbf{b} \cdot \gamma)\mathbf{b} = \mathbf{0}, \tag{63}$$

and the strong-ellipticity conditions (31) again yield $\gamma = \mathbf{0}$, which again is energetically optimal. Then, because $\mathbf{c}$ is positive definite, it follows from $(49)_1$ that $\mathbf{e} = \mathbf{0}$, yielding

$$\overline{\mathbf{E}} = \varepsilon - (tr\varepsilon)\mathbf{k} \otimes \mathbf{k} \tag{64}$$

and

$$\mathbf{d} = \lambda\, \mathbf{n}, \quad \text{with} \quad \lambda = \alpha^{-1}\,. \tag{65}$$

Thus, we have derived the well known Kirchhoff-Love hypothesis with thickness distension as the asymptotic leading-order approximation. Further, $Q(\bar{\mathbf{E}})$ is then determined entirely by $\nabla\mathbf{r}$. We combine (44) and $(49)_2$, reaching

$$\frac{1}{2}(\lambda^2 - 1) = \bar{E} = -tr\varepsilon + O(|\mathbf{E}|^2)\,. \tag{66}$$

Accordingly λ should be replaced by unity in the coefficient of h^3 in the energy (57).

To elaborate, from $(39)_2$ and (65) we have that

$$\mathbf{F}' = \lambda\, \nabla\mathbf{n} + \mathbf{n} \otimes \nabla\, \lambda + \mathbf{g} \otimes \mathbf{k}, \tag{67}$$

where $\nabla\mathbf{n}$ is the referential gradient, defined by $d\mathbf{n} = (\nabla\mathbf{n})d\mathbf{u}$. Let $\mathbf{b}$ be the curvature tensor of the deformed surface ω; this is the symmetric 2-tensor, defined by $d\mathbf{n} = -\mathbf{b}d\mathbf{r}$, that maps the tangent plane T_ω at a particular material point to itself. Thus,

$$\nabla\mathbf{n} = -\mathbf{b}(\nabla\mathbf{r}). \tag{68}$$

In the course of arriving at (57), to be consistent with (53), we have approximated $\mathbf{F}$ by $\mathbf{R}$. To this order of approximation, $\mathbf{E}$ vanishes and $\lambda = 1$. Moreover, with

$$\mathbf{R} = \mathbf{R1} + \mathbf{Rk} \otimes \mathbf{k}, \tag{69}$$

the same approximation, in combination with $(39)_1$, gives

$$\mathbf{R1} \simeq \nabla\mathbf{r} \quad \text{and} \quad \mathbf{Rk} = \mathbf{n}. \tag{70}$$

Then the consistent-order approximation to $\mathbf{R}^t\mathbf{F}'$ is

$$\mathbf{R}^t\mathbf{F}' \simeq \kappa + \mathbf{k} \otimes \nabla\lambda + \mathbf{R}^t\mathbf{g} \otimes \mathbf{k}, \tag{71}$$

where

$$\kappa = -(\nabla\mathbf{r})^t\mathbf{b}(\nabla\mathbf{r}) \tag{72}$$

is a symmetric 2-tensor on Ω'.

Recalling that consistency of (59) with bulk incompressibility requires that $\mathbf{R}^t\mathbf{F}'$ be deviatoric at leading order, we impose $tr(\mathbf{R}^t\mathbf{F}') = 0$ and conclude that

$$\mathbf{k} \cdot \mathbf{R}^t\mathbf{g} \simeq -tr\kappa. \tag{73}$$

This agrees with the consistent-order approximation to (45) on noting that $\mathbf{F}^* \cdot \nabla\mathbf{d} = \mathbf{F}^*\mathbf{1} \cdot \nabla\mathbf{d}$ with $\mathbf{F}^* \simeq \mathbf{R}$; namely,

$$\mathbf{n} \cdot \mathbf{g} \simeq -\mathbf{R1} \cdot (\nabla\mathbf{n} + \mathbf{n} \otimes \nabla\lambda), \tag{74}$$

in which $\mathbf{R1} \cdot \mathbf{n} \otimes \nabla\lambda = \mathbf{n}\nabla(\nabla\mathbf{r})\nabla\lambda$ vanishes because $(\nabla\mathbf{r})\nabla\lambda \in T_\omega$. Writing

$$\mathbf{R}^t\mathbf{g} = \mathbf{1}(\mathbf{R}^t\mathbf{g}) + (\mathbf{k} \cdot \mathbf{R}^t\mathbf{g})\mathbf{k}, \tag{75}$$

we then have

$$\mathbf{R}^t\mathbf{F}' \simeq \kappa - (tr\kappa)\mathbf{k} \otimes \mathbf{k} + \mathbf{k} \otimes \nabla\lambda + \mathbf{1}(\mathbf{R}^t\mathbf{g}) \otimes \mathbf{k}. \tag{76}$$

The energy (57) involves only the symmetric part:

$$Sym(\mathbf{R}^t\mathbf{F}') \simeq \kappa - (tr\kappa)\mathbf{k} \otimes \mathbf{k} + Sym(\mu \otimes \mathbf{k}), \tag{77}$$

where

$$\mu = \mathbf{1}(\mathbf{R}^t\mathbf{g}) + \nabla\ \lambda\ . \tag{78}$$

This has a structure similar to (51).

Proceeding as in the foregoing, we seek $\mathbf{1}(\mathbf{R}^t\mathbf{g})$ (equivalently, $\mathbf{f}$) that renders the energy stationary at fixed $\nabla\mathbf{r}$ and $\mathbf{e}$. With reference to (60), this implies that at leading order the former should satisfy

$$\dot{\mu} \cdot (\mathscr{C}[\mathbf{R}^t\mathbf{F}'])\mathbf{k} = 0 \tag{79}$$

for all $\dot{\mu} \in \Omega'$; i.e.,

$$\mathbf{1}(\mathscr{C}[\mathbf{R}^t\mathbf{F}'])\mathbf{k} = \mathbf{0}, \tag{80}$$

which is easily seen to reduce to (62) or (63), with γ replaced by μ, for transversely isotropic or orthotropic materials respectively. We conclude that $\mu = \mathbf{0}$, and again strong ellipticity implies that this solution is energetically optimal (Steigmann, 2010). Thus,

$$Sym(\mathbf{R}^t\mathbf{F}') \simeq \kappa - (tr\kappa)\mathbf{k} \otimes \mathbf{k}, \tag{81}$$

and the strain energy (57) reduces to

$$W = hQ^*(\varepsilon) + \frac{1}{12}h^3Q^*(\kappa), \tag{82}$$

where, for any symmetric 2-tensor α on Ω',

$$Q^*(\alpha) = Q(\alpha - (tr\alpha)\mathbf{k} \otimes \mathbf{k})\,. \tag{83}$$

This is an additive decomposition of the strain energy into pure membrane and bending energies, as in Koiter's well established model (Koiter, 1960, 1966) for isotropic materials undergoing finite deformations with small midplane strains. Indeed, (82) provides the extension of Koiter's energy to incompressible transversely isotropic or orthotropic materials. It is determined entirely by the 1st and 2nd gradients of the midsurface deformation $\mathbf{r}(\mathbf{u})$.

Remark: Our procedure for eliminating $\mathbf{e}$ and $\mathbf{f}$ relied on asymptotic estimates of the associated stationarity conditions at leading order in h and at fixed midplane deformation. On the other hand, the leading-order stationarity condition for the energy (82) furnishes membrane theory, which is known to be ill-posed as a minimization problem due to the failure of $Q^*(\varepsilon)$ to satisfy the operative Legendre-Hadamard necessary condition. This in turn is due to the presence of compressive in-plane 2nd Piola-Kirchhoff stresses in the stress-deformation relation derived from $Q^*(\varepsilon)$ (Steigmann, 1986; Shirani and Steigmann, 2019). In this case a well-posed formulation is achieved on replacing $Q^*(\varepsilon)$ by its *quasiconvexification* (Pipkin, 1994; Dacarogna, 1989; Le Dret and Raoult, 1996), which automatically furnishes equilibria having no compressive stress. These equilibria also

furnish the least possible membrane energy that can be attributed to a given midplane deformation. This model was adapted to anisotropic membranes in Pipkin (1994) and further specialized to orthotropic bio-elastic membranes in Atai and Steigmann (2014). However, the relaxed membrane problem lacks the intrinsic length scale h required to resolve the spatial distribution of wrinkle patterns. For this reason we retain the full energy (82) in the ensuing variational treatment. In Section 5, we show that this procedure also yields an effective regularization of membrane theory.

For transversely isotropic laminae, (22) and (83) may be used to obtain

$$Q^*(\alpha) = \mu_T[\alpha\cdot\alpha + (tr\alpha)^2] + 2(\mu_L - \mu_T)\alpha\mathbf{a}\cdot\alpha\mathbf{a} + \frac{1}{2}\beta(\mathbf{a}\cdot\alpha\mathbf{a})^2\,. \tag{84}$$

The derivative Q^*_α, needed in Section 4, is

$$Q^*_\alpha = 2\mu_T[\alpha + (tr\alpha)\mathbf{1}] + 2(\mu_L - \mu_T)(\alpha\mathbf{a}\otimes\mathbf{a} + \mathbf{a}\otimes\alpha\mathbf{a}) + \beta(\mathbf{a}\cdot\alpha\mathbf{a})\mathbf{a}\otimes\mathbf{a}\,. \tag{85}$$

For orthotropic laminae, we find, using (23), that

$$\begin{aligned} Q^*(\alpha) &= \mu[\alpha\cdot\alpha + (tr\alpha)^2] + 2\mu_a\alpha\mathbf{a}\cdot\alpha\mathbf{a} + 2\mu_b\alpha\mathbf{b}\cdot\alpha\mathbf{b} + \frac{1}{2}\beta_a(\mathbf{a}\cdot\alpha\mathbf{a})^2 \\ &+ \frac{1}{2}\beta_b(\mathbf{b}\cdot\alpha\mathbf{b})^2 + \beta_{ab}(\mathbf{a}\cdot\alpha\mathbf{a})(\mathbf{b}\cdot\alpha\mathbf{b}), \end{aligned} \tag{86}$$

with derivative

$$\begin{aligned} Q^*_\alpha &= 2\mu[\alpha + (tr\alpha)\mathbf{1}] + 2\mu_a(\alpha\mathbf{a}\otimes\mathbf{a} + \mathbf{a}\otimes\alpha\mathbf{a}) + 2\mu_b(\alpha\mathbf{b}\otimes\mathbf{b} + \mathbf{b}\otimes\alpha\mathbf{b}) \\ &+ [\beta_a(\mathbf{a}\cdot\alpha\mathbf{a}) + \beta_{ab}(\mathbf{b}\cdot\alpha\mathbf{b})]\mathbf{a}\otimes\mathbf{a} + [\beta_{ab}(\mathbf{a}\cdot\alpha\mathbf{a}) + \beta_b(\mathbf{b}\cdot\alpha\mathbf{b})]\mathbf{b}\otimes\mathbf{b}\,. \end{aligned} \tag{87}$$

3.2. Positive-definiteness conditions

Inequality (18), combined with (83), implies that $Q^*(\alpha)$ is positive definite. This in turn imposes restrictions on the moduli, which we pause to derive here. To this end we decompose α in the form

$$\alpha = \alpha_{aa}\mathbf{a}\otimes\mathbf{a} + \alpha_{bb}\mathbf{b}\otimes\mathbf{b} + \alpha_{ab}(\mathbf{a}\otimes\mathbf{b} + \mathbf{b}\otimes\mathbf{a})\,. \tag{88}$$

We combine this with (84) and (85) to deduce, after some some algebra, that for both the transversely isotropic and orthotropic laminae,

$$Q^*(\alpha) = A\alpha_{aa}^2 + B\alpha_{bb}^2 + 2C\alpha_{aa}\alpha_{bb} + D\alpha_{ab}^2, \tag{89}$$

where $A - D$ depend only on the moduli. This is sum of two independent quadratic forms. Accordingly, $Q^*(\alpha)$ is positive definite if and only if both quadratic forms are positive definite. Necessary and sufficient conditions are

$$AB - C^2 > 0, \quad B > 0 \quad \text{and} \quad D > 0\,. \tag{90}$$

For transversely isotropic laminae, we derive

$$A = 2\mu_L + \frac{1}{2}\beta, \quad B = 2\mu_T, \quad C = \mu_T \quad \text{and} \quad D = 2\mu_L, \tag{91}$$

and $Q^*(\cdot)$ is then positive definite if and only if

$$\mu_T > 0, \quad \beta > \mu_T - 4\mu_L \quad \text{and} \quad \mu_L > 0\,. \tag{92}$$

For orthotropic laminae, we find that

$$A = 2(\mu + \mu_a) + \frac{1}{2}\beta_a, \quad B = 2(\mu + \mu_b) + \frac{1}{2}\beta_b, \quad C = \mu + \frac{1}{2}\beta_{ab} \quad \text{and} \quad D = 2(\mu + \mu_a + \mu_b), \tag{93}$$

and $Q^*(\cdot)$ is positive definite if and only if

$$\mu + \mu_a + \mu_b > 0, \quad 4(\mu + \mu_b) + \beta_b > 0 \quad \text{and} \quad [4(\mu + \mu_a) + \beta_a][4(\mu + \mu_b) + \beta_b] > 4(\mu + \frac{1}{2}\beta_{ab})^2\,. \tag{94}$$

3.3. Laminated plates

Our framework may be used to construct a two-dimensional model of laminates. The utility of such models in structural mechanics is of course well known, but the model is also applicable to the mitral valve, for example, which is thought to have a layered structure (Wenk et al., 2012; Zhang et al., 2016). We confine attention to laminates consisting of two laminae of the kind considered in the foregoing, and identify the plane Ω, on which $\varsigma = 0$, with the interface between them. The *upper* lamina occupies the interval $\varsigma \in (0, \eta h]$ and the *lower* lamina the interval $\varsigma \in [-(1-\eta)h, 0)$, where $\eta \in [0,1]$ is a fixed constant and h is again the thickness of the laminate. The areal energy density on Ω is then given by (compare (34))

$$\begin{aligned}&\int_0^{\eta h} U_+(\widetilde{\mathbf{E}}_+(\mathbf{u} + \varsigma\mathbf{k}))d\varsigma + \int_{-(1-\eta)h}^{0} U_-(\widetilde{\mathbf{E}}_-(\mathbf{u} + \varsigma\mathbf{k}))d\varsigma \\ &= h[\eta U_+ + (1-\eta)U_-] + \frac{1}{2}h^2[\eta^2 U'_+ - (1-\eta)^2 U'_-] \\ &+ \frac{1}{6}h^3[\eta^3 U''_+ + (1-\eta)^3 U''_-] + o(h^3),\end{aligned} \tag{95}$$

where again Leibniz' Rule has been combined with a Taylor expansion in each integral (Steigmann, 2012) and the subscripts ± pertain to the upper and lower laminae respectively.

Estimating the coefficients of h, h^2 and h^3 at leading order in $|\mathbf{E}_+|$ in the upper lamina and $|\mathbf{E}_-|$ in the lower lamina, we arrive at (56), with

$$W = h[\eta Q_+(\overline{\mathbf{E}}_+) + (1-\eta)Q_-(\overline{\mathbf{E}}_-)] + \frac{1}{2}h^2 \{\eta^2 \mathscr{C}_+[\overline{\mathbf{E}}_+] \cdot \mathbf{R}_+^t \mathbf{F}'_+ - (1-\eta)^2 \mathscr{C}_-[\overline{\mathbf{E}}_-] \cdot \mathbf{R}_-^t \mathbf{F}'_-\} + \frac{1}{3}h^3[\eta^3 Q_+(\mathbf{R}_+^t \mathbf{F}'_+) + (1-\eta)^3 Q_-(\mathbf{R}_-^t \mathbf{F}'_-)], \tag{96}$$

where

$$\overline{\mathbf{E}}_\pm = \varepsilon - (tr\varepsilon)\mathbf{k} \otimes \mathbf{k} + Sym(\gamma_\pm \otimes \mathbf{k}) \tag{97}$$

and

$$Sym(\mathbf{R}_\pm^t \mathbf{F}'_\pm) = \kappa - (tr\kappa)\mathbf{k} \otimes \mathbf{k} + Sym(\mu_\pm \otimes \mathbf{k})\,. \tag{98}$$

Here, we assume the laminae to be perfectly bonded at the plane Ω, each then having a common interfacial deformation $\mathbf{r}(\mathbf{u}) = \tilde{\chi}_{\pm\,|\,\Omega}$. This implies that ε and κ, which are determined by the derivatives of $\mathbf{r}(\mathbf{u})$, are also common to the two laminae.

The leading-order asymptotic analysis culminating in (60), (79) may be applied to the fields $\gamma_\pm (= \mathbf{c}\mathbf{e}_\pm)$ separately to conclude, as there, that $\gamma_\pm$ (and hence $\mathbf{e}_\pm$) vanish, yielding $\bar{\mathbf{E}}_\pm = \bar{\mathbf{E}}$, given by (64). Thus the restriction of the strain to Ω is the same for both laminae. In view of the structure of (84) and (86), and because the fiber axes $\mathbf{a}_\pm$ and $\mathbf{b}_\pm$ are assumed to be orthogonal to the unit normal, $\mathbf{k}$, to Ω′, it follows that $\mathscr{C}_\pm[\bar{\mathbf{E}}_\pm] \cdot \mathbf{R}_\pm^t \mathbf{F}'_\pm$ do not involve $\mu_\pm$. Accordingly, the asymptotic procedure culminating in (80) applies here as well, and with the same conclusion; namely, that $\mu_\pm$ vanish. Finally, the areal energy density reduces to

$$W = h[\eta Q_+(\overline{\mathbf{E}}) + (1-\eta)Q_-(\overline{\mathbf{E}})] + \frac{1}{2}h^2\{\eta^2 \mathscr{C}_+[\overline{\mathbf{E}}] - (1-\eta)^2 \mathscr{C}_-[\overline{\mathbf{E}}]\} \cdot Sym(\mathbf{R}^t \mathbf{F}') + \frac{1}{3}h^3[\eta^3 Q_+(\mathbf{R}^t \mathbf{F}') + (1-n)^3 Q_-(\mathbf{R}^t \mathbf{F}')], \tag{99}$$

where $\bar{\mathbf{E}}$ and $Sym(\mathbf{R}^t \mathbf{F}')$ are given respectively by (64) and (81). This energy is again fully specified by the derivatives of the deformation $\mathbf{r}(\mathbf{u})$ of the interfacial plane. It may be expressed in terms of the reduced energy Q^* defined in (83); thus,

$$W = h[\eta Q_+^*(\varepsilon) + (1-\eta)Q_-^*(\varepsilon)] + \frac{1}{2}h^2\{\eta^2 \mathscr{C}_+[\overline{\mathbf{E}}] - (1-\eta)^2 \mathscr{C}_-[\overline{\mathbf{E}}]\} \cdot Sym(R^t \mathbf{F}') + \frac{1}{3}h^3[\eta^3 Q_+^*(\kappa)(1-\eta)^3 Q_-^*(\kappa)]\,. \tag{100}$$

The coefficient of h^2 in this expression couples the extensional and bending strains ε and κ. It vanishes if the laminate is apportioned to both laminae equally ($\eta = 1/2$), and if they have identical properties; the energy reduces, in this case, to (82), as expected.

4. Equilibrium

Consider a one-parameter family $\mathbf{r}(\mathbf{u}; \epsilon)$ of deformations and let $\mathbf{v}(\mathbf{u}) = \dot{\mathbf{r}}$, where $\dot{\mathbf{r}} = \partial \mathbf{r}(\mathbf{u}; \epsilon) \big/ \partial \epsilon \,|_{\epsilon = 0}$; this is the virtual velocity field. We identify equilibria with those deformations $\mathbf{r}(\mathbf{u}) = \mathbf{r}(\mathbf{u};0)$ that satisfy the virtual-power statement

$$\dot{E} = P \tag{101}$$

for all kinematically admissible $\mathbf{v}$, where E is the strain energy (56) and

$$\dot{E} = \int_{\Omega} \dot{W}\, da \tag{102}$$

in which the superposed dot is the derivative with respect to ϵ at the equilibrium state $\epsilon = 0$; and P, the form of which is made explicit below, is the virtual power supplied by an external agency. The meaning of kinematic admissibility in this context is discussed below. Here we observe, from $(49)_3$, (81) and (82) or (100), that the strain energy W depends on the deformation through its first and second spatial derivatives on Ω. Therefore, plate theory is subsumed under second-grade elasticity theory (Toupin, 1962, 1964). Indeed, this circumstance affords a much clearer conceptual framework for plate theory than is typically found in the text and monograph literatures.

To elaborate, we adopt a Cartesian-coordinate parametrization of Ω. Thus, with $\mathbf{u} = u_\alpha \mathbf{e}_\alpha$, where u_α are the coordinates, we have $\mathbf{r}(\mathbf{u}) = r_i(u_\alpha)\mathbf{e}_i$, where $r_i(u_\alpha) = \mathbf{e}_i \cdot \mathbf{r}(u_\beta \mathbf{e}_\beta)$, and

$$\nabla \mathbf{r} = \mathbf{a}_\alpha \otimes \mathbf{e}_\alpha, \quad \text{with} \quad \mathbf{a}_\alpha = r_{i,\alpha}\mathbf{e}_i; \tag{103}$$

and, from $(49)_3$,

$$\varepsilon = \varepsilon_{\alpha\beta}\mathbf{e}_\alpha \otimes \mathbf{e}_\beta, \quad \text{with} \quad \varepsilon_{\alpha\beta} = \frac{1}{2}(a_{\alpha\beta} - \delta_{\alpha\beta}), \tag{104}$$

where $a_{\alpha\beta} = r_{i,\alpha} r_{i,\beta}$ is the metric induced by the (convected) coordinates on ω; here $\delta_{\alpha\beta}$ is the Kronecker delta. The metric furnishes the representation

$$\mathbf{c} = a_{\alpha\beta}\mathbf{e}_\alpha \otimes \mathbf{e}_\beta \tag{105}$$

of the surface Cauchy-Green tensor via $(46)_2$, and this is positive definite on Ω' by virtue of the positive definiteness of the three-dimensional Cauchy-Green tensor $(46)_1$. The matrix $(a_{\alpha\beta})$ is accordingly positive definite.

From the Gauss and Weingarten equations of differential geometry (Flügge, 1972), we also have

$$r_{i;\alpha\beta} = n_i b_{\alpha\beta}, \tag{106}$$

where n_i are the components of the unit normal $\mathbf{n}$ to T_ω, $b_{\alpha\beta}$ are the components of the curvature tensor thereon, and

$$r_{i;\,\alpha\beta} = r_{i,\,\alpha\beta} - \Gamma^{\mu}_{\alpha\beta}\, r_{i,\,\mu} \tag{107}$$

is the covariant derivative on ω, in which $\Gamma^{\mu}_{\alpha\beta}$ are the Christoffel symbols, given by

$$\Gamma^{\lambda}_{\alpha\beta} = \frac{1}{2} a^{\lambda\mu}(a_{\alpha\mu,\,\beta} + a_{\beta\mu,\,\alpha} - a_{\alpha\beta,\,\mu}), \tag{108}$$

with $(a^{\lambda\mu}) = (a_{\lambda\mu})^{-1}$. The curvature tensor is $\mathbf{b} = b_{\alpha\beta}\mathbf{a}^{\alpha} \otimes \mathbf{a}^{\beta}$, where $\mathbf{a}^{\alpha} = a^{\alpha\beta}\mathbf{a}_{\beta}$, and the surface normal may be computed from the deformation using the formula $\epsilon_{\alpha\beta}\mathbf{n} = \mathbf{a}_{\alpha} \times \mathbf{a}_{\beta}$, where $\epsilon_{\alpha\beta} = \sqrt{a}e_{\alpha\beta}$ in which $a = \det(a_{\alpha\beta})$ and $e_{\alpha\beta}$ is the permutation symbol ($e_{12} = -e_{21} = 1$, $e_{11} = e_{22} = 0$). From (106), (107) and $n_i r_{i,\alpha} = 0$ we have

$$b_{\alpha\beta} = n_i r_{i,\,\alpha\beta}, \tag{109}$$

and (72), (103) combine to give

$$\kappa = -b_{\alpha\beta}\mathbf{e}_{\alpha} \otimes \mathbf{e}_{\beta}. \tag{110}$$

Recall that the strain energy is a function, F say, of the components $r_{i,\alpha}$ and $r_{i,\alpha\beta}$. Then,

$$\dot{W} = N_{i\alpha} v_{i,\,\alpha} + M_{i\alpha\beta} v_{i,\,\alpha\beta}, \tag{111}$$

with

$$N_{i\alpha} = \partial F / \partial r_{i,\,\alpha} \quad \text{and} \quad M_{i\alpha\beta} = M_{i\beta\alpha} = \partial F / \partial r_{i,\,\alpha\beta}. \tag{112}$$

We define a 2-vector φ with components

$$\varphi_{\alpha} = T_{i\alpha} v_i + M_{i\alpha\beta} v_{i,\,\beta}, \quad \text{where} \quad T_{i\alpha} = N_{i\alpha} - M_{i\alpha\beta,\,\beta}. \tag{113}$$

Then,

$$\dot{W} = \varphi_{\alpha,\,\alpha} - v_i T_{i\alpha,\,\alpha}, \tag{114}$$

and it follows from the Green-Stokes theorem that

$$\dot{E} = \int_{\partial\Omega} \varphi_{\alpha} \nu_{\alpha} ds - \int_{\Omega} v_i T_{i\alpha,\,\alpha} da, \tag{115}$$

where ν_{α} is the rightward unit normal to the edge $\partial\Omega$, traversed counter-clockwise.

Let $u_{\alpha}(s)$ be the arclength parametrization of $\partial\Omega$. The unit tangent to $\partial\Omega$ is the vector with components $\tau_{\alpha} = du_{\alpha}/ds$, and $\nu_{\alpha} = e_{\alpha\beta}\tau_{\beta}$. We use these with $\delta_{\alpha\beta} = \tau_{\alpha}\tau_{\beta} + \nu_{\alpha}\nu_{\beta}$ to decompose the derivatives $v_{i,\beta} (= v_{i,\alpha}\delta_{\alpha\beta})$ on $\partial\Omega$ in the form

$$v_{i,\beta} = T_\beta v_i' + \nu_\beta v_{i,\nu}, \tag{116}$$

where $v_i'(s) = \tau_\alpha v_{i,\alpha} = dv_i(\mathbf{u}(s)) \big/ ds$ and $v_{i,\nu}(s) = \nu_\alpha v_{i,\alpha}$ respectively are the independent tangential and normal derivatives of v_i on $\partial\Omega$. Substituting into $(113)_1$ and (115), we find that

$$\begin{aligned} \int_{\partial\Omega} \varphi_\alpha \nu_\alpha ds &= \int_{\partial\Omega} \{(T_{i\alpha}\nu_\alpha - (M_{i\alpha\beta}\nu_\alpha\tau_\beta)')v_i + M_{i\alpha\beta}\nu_\alpha\nu_\beta v_{i,\nu}\} ds \\ &- \sum_n [M_{i\alpha\beta}\nu_\alpha\tau_\beta]_{(n)} v_{i(n)}, \end{aligned} \tag{117}$$

where the square bracket refers to the forward jump as a corner of the boundary is traversed. Thus, $[\cdot] = (\cdot)_+ - (\cdot)_-$, where the subscripts $_\pm$ identify the limits as a corner located at arclength station s is approached through larger and smaller values of arclength, respectively. The sum accounts for the contributions from all corners. Here we assume the boundary to be piecewise smooth in the sense that its tangent $\boldsymbol{\tau}$ is piecewise continuous.

It follows from (101) that admissible virtual powers have the form

$$P = \int_\Omega g_i v_i da + \int_{\partial\Omega_t} t_i v_i ds + \int_{\partial\Omega_m} m_i v_{i,\nu} ds + \sum_* f_{i(n)} v_{i(n)}, \tag{118}$$

where g_i, t_i, m_i and $f_{i(n)}$ respectively are the distributed force, the edge traction, the double force, and the corner force. The notion of double force figures prominently in 2nd-grade elasticity theory (Toupin, 1962, 1964). Here, $\partial\Omega_t$ and $\partial\Omega_m$ respectively are parts of $\partial\Omega$ where r_i and $r_{i,\nu}$ are not assigned, and the starred sum includes only the corners where position is not assigned. We suppose that r_i and $r_{i,\nu}$ are assigned, and hence that v_i and $v_{i,\nu}$ vanish, on $\partial\Omega \setminus \partial\Omega_t$ and $\partial\Omega \setminus \partial\Omega_m$, respectively, and that position is assigned at the corners not included in the starred sum, so that $v_{i(n)}$ vanishes there. For our present purposes, these restrictions on the virtual velocity constitute the definition of kinematic admissibility. The fundamental lemma then yields the Euler-Lagrange equations

$$T_{i\alpha,\alpha} + g_i = 0 \quad \text{in} \quad \Omega, \tag{119}$$

and

$$t_i = T_{i\alpha}\nu_\alpha - (M_{i\alpha\beta}\nu_\alpha\tau_\beta)', \quad m_i = M_{i\alpha\beta}\nu_\alpha\nu_\beta \quad \text{and} \quad f_{i(n)} = -[M_{i\alpha\beta}\nu_\alpha\tau_\beta]_{(n)} \tag{120}$$

on $\partial\Omega_t$, $\partial\Omega_m$ and at the n^{th} corner, respectively.

In conventional plate theory, it is customary to specify a couple $\mathbf{c}$ on part of the boundary. This is related to the double force by $\mathbf{c} = \mathbf{r}_{,\nu} \times \mathbf{m}$ (Steigmann, 2018), where $\mathbf{r}_{,\nu} = r_{i,\nu}\mathbf{e}_i$ and $\mathbf{m} = m_i\mathbf{e}_i$. The couple and double force are not equivalent, however, because the former is sensitive only to the part of the latter that is perpendicular to $\mathbf{r}_{,\nu}$. It follows that, in general, specification of the couple is not consistent with the variational statement (101).

We use (82) to deduce the structure of the response functions $N_{i\alpha}$ and $M_{i\alpha\beta}$ for a single lamina. Thus,

$$\dot{W} = hQ_{\varepsilon}^{*} \cdot \dot{\varepsilon} + \frac{1}{12} h^{3} Q_{\kappa}^{*} \cdot \dot{\kappa} . \tag{121}$$

Equivalently,

$$\dot{W} = \sum_{\alpha\beta} \dot{\varepsilon}_{\alpha\beta} + M_{\alpha\beta} \dot{b}_{\alpha\beta}, \tag{122}$$

where

$$\sum_{\alpha\beta} = hQ_{\varepsilon}^{*} \cdot \mathbf{e}_{\alpha} \otimes \mathbf{e}_{\beta} \quad \text{and} \quad M_{\alpha\beta} = -\frac{1}{12} h^{3} Q_{\kappa}^{*} \cdot \mathbf{e}_{\alpha} \otimes \mathbf{e}_{\beta} . \tag{123}$$

and the derivatives Q_{ε}^{*}, Q_{κ}^{*} are given by (85) or (87). Here we use $(104)_2$ to compute the variation

$$\dot{\varepsilon}_{\alpha\beta} = \frac{1}{2} (r_{i,\alpha} v_{i,\beta} + v_{i,\alpha} r_{i,\beta}) . \tag{124}$$

To compute the variation $\dot{b}_{\alpha\beta}$, we first take the variation of (106), reaching

$$v_{i,\alpha\beta} = \Gamma_{\alpha\beta}^{\mu} v_{i,\mu} + \dot{\Gamma}_{\alpha\beta}^{\mu} r_{i,\mu} + b_{\alpha\beta} \dot{n}_{i} + \dot{b}_{\alpha\beta} n_{i}, \tag{125}$$

and then contract with n_i to obtain

$$\dot{b}_{\alpha\beta} = n_{i} (v_{i,\alpha\beta} - \Gamma_{\alpha\beta}^{\mu} v_{i,\mu}) . \tag{126}$$

Because the energy (82) is valid to leading order in the strain, we adopt the consistent-order approximation $(a_{\alpha\beta})^{-1} = \delta_{\alpha\beta} + O(|\varepsilon|)$. From (108) we then have

$$\Gamma_{\alpha\beta}^{\mu} = \overline{\Gamma}_{\mu\alpha\beta} + O(|\varepsilon|), \tag{127}$$

where

$$\overline{\Gamma}_{\mu\alpha\beta} = \varepsilon_{\alpha\mu,\beta} + \varepsilon_{\beta\mu,\alpha} - \varepsilon_{\alpha\beta,\mu} . \tag{128}$$

To the same order of approximation, the unit normal $\mathbf{n} = n_k \mathbf{e}_k$ to the deformed surface is given by

$$e_{\alpha\beta} n_{k} = e_{ijk} r_{i,\alpha} r_{j,\beta}, \tag{129}$$

where $e_{\alpha\beta}$ and e_{ijk} respectively are the two- and three-dimensional permutation symbols. Combining these results with (111) and (122), we arrive at

$$M_{i\alpha\beta} = n_i M_{\alpha\beta} \quad \text{and} \quad N_{i\alpha} = r_{i,\beta} \sum_{\beta\alpha} - M_{i\beta\mu}\, \overline{\Gamma}_{\alpha\beta\mu}\,, \tag{130}$$

in which the non-standard term $M_{i\beta\mu}\, \overline{\Gamma}_{\alpha\beta\mu}$ arises from the use of partial derivatives rather than the customary covariant derivatives (see (107)) on the deformed surface (Ciarlet, 2005). We note that it is a purely nonlinear term and hence absent in linear plate theory.

The reduction of laminate theory proceeds along entirely similar lines and is therefore not made explicit. The only adjustments to the foregoing are that the definitions of $\Sigma_{\alpha\beta}$ and $M_{\alpha\beta}$ are to be based on (100) rather than (82).

Eqs. (103) may be substituted into $(113)_2$, (119) and (120) to derive expressions for the distributed force, the traction, the double force and the corner forces. In particular, the double force assumes the form

$$m_i = M n_i, \quad \text{with} \quad M = M_{\alpha\beta}\nu_\alpha \nu_\beta\,. \tag{131}$$

This implies that the edge couple, $\mathbf{c} = \mathbf{r}_{,\nu} \times \mathbf{m}$, is tangential to the deformed surface, and that it vanishes if and only if the double force vanishes.

5. Gradient flow and dynamic relaxation

We apply the foregoing to the analysis of problems in which there is no distributed load over the surface of the plate ($g_i = 0$) and parts $\partial\Omega_c$ and $\partial\Omega_f$ of the boundary are either clamped (r_i and $r_{i,\nu}$ assigned) or free ($t_i = 0$ and $m_i = 0$), respectively. In all cases the corners of the plate are the endpoints of clamped segments, so that r_i are assigned there. The normal-tangential decomposition (116) implies that the full gradient $r_{i,\alpha}$, is effectively assigned on a clamped boundary. This follows from the fact that the specification of $r_i(s)$ yields the tangential derivatives $r_i'(s)$. The specification of the normal derivatives $r_{i,\nu}(s)$ may be interpreted in terms of an assigned position field in a narrow seam of width w, say, welded to the boundary. If ν is the normal coordinate on the edge, then $r_i(s, \nu) = r_i(s) + \nu r_{i,\nu}(s) + o(\nu)$ for $0 \le \nu \le w$. Dividing by ν and passing to the limit, we conclude that specification of the normal derivative furnishes the leading-order model for the specification of position $r_i(s,\nu)$ in the adjoining seam.

With the foregoing conditions in effect, the virtual-power statement (101) reduces simply to $\dot{E} = 0$. Moreover, the problem is trivially conservative, with E playing the role of the potential energy. According to the energy criterion for conservative problems, stable equilibria $\mathbf{r}(\mathbf{u})$ may be identified with minimizers of this energy.

An effective method for treating problems of this kind is the so-called *gradient-flow* algorithm, in which the stationarity condition $\dot{E} = 0$ is replaced by the following artificial first-order dynamical problem, with $\mathbf{v}(\mathbf{u}, \epsilon) = \partial\mathbf{r}(\mathbf{u}; \epsilon)/\partial\epsilon$:

$$c v_i = T_{i\alpha,\alpha} \quad \text{in} \quad \Omega\,, \tag{132}$$

and

$$-cv_i = T_{i\alpha}\nu_\alpha - (M_{i\alpha\beta}\nu_\alpha\tau_\beta)' \quad \text{on} \quad \partial\Omega_f\,, \quad \text{and} \quad -cv_{i,\nu} = M_{i\alpha\beta}\nu_\alpha\nu_\beta \quad \text{on} \quad \partial\Omega_f\,, \tag{133}$$

with c a positive constant and with $v_i = 0$ and $v_{i,\alpha} = 0$ on $\partial\Omega_c = \partial\Omega \setminus \partial\Omega_f$. With reference to (115) and (117), this yields

$$\frac{\partial}{\partial\epsilon}E[\mathbf{r}(\mathbf{u};\epsilon)] = -c^{-1}\left(\int_\Omega |\mathbf{g}|^2 da + \int_{\partial\Omega_f} |\mathbf{t}|^2 ds + \int_{\partial\Omega_f} |\mathbf{m}|^2 ds\right), \tag{134}$$

where the components of **g**, **t** and **m** are given respectively by (119) and $(120)_{1,2}$.

Thus, $\partial E[\mathbf{r}(\mathbf{u};\epsilon)]/\partial\epsilon \le 0$, with equality (and hence E stationary) if and only if the equilibrium conditions are satisfied. Forward integration of (132) and (133) in 'ϵ - time' with arbitrary initial conditions thus generates an energy-minimizing sequence $\mathbf{r}_n(\mathbf{u}) = \mathbf{r}(\mathbf{u};\epsilon_n)$, where ϵ_n are discrete values of ϵ; that is, $E[\mathbf{r}_{n+1}(\mathbf{u})] < E[\mathbf{r}_n(\mathbf{u})]$. This sequence converges to a minimizer provided that the energy is lower semi-continuous. This in turn is guaranteed by the condition of quasiconvexity of the areal strain-energy function W with respect to the 2nd gradient $r_{i,\alpha\beta}$ (Ball et al., 1981). The relevant term is $Q^*(\boldsymbol{\kappa})$, in which $\boldsymbol{\kappa}$ depends on $r_{i,\alpha\beta}$, linearly (cf. (109) and (110)). Thus W is a non-negative, quadratic and hence convex function of $r_{i,\alpha\beta}$. It is not strictly convex, however, because while Q^* is a positive-definite function of $\boldsymbol{\kappa}$, the latter is insensitive to the part of $r_{i,\alpha\beta}$ orthogonal to n_i. Nevertheless, convexity is sufficient for quasiconvexity and hence for lower semicontinuity, which in turn ensures the convergence of the gradient-flow algorithm. It is in this sense that plate theory furnishes a regularization of pure membrane theory.

The foregoing statements are not sufficiently precise to be entirely equivalent to what has been proved. We refer to Ball et al. (1981) for detailed statements and proofs of the relevant theorems.

In practice, the rate of convergence of the gradient-flow algorithm is rather slow. To address this, we instead use the *dynamic relaxation* method (Shugar, 1990; Topping and Khan, 1994; Rezaiee-pajand et al., 2011), which entails the addition of an artificial inertia to (132). This is motivated by the fact that, in the linear theory of damped vibrations, inertia hastens the transient response of the system and its approach to equilibrium. Thus we replace (132) by

$$\rho\dot{v}_i + cv_i = T_{i\alpha,\alpha} \quad \text{in} \quad \Omega\,, \tag{135}$$

where $\dot{\mathbf{v}}(\mathbf{u},\epsilon) = \partial^2\mathbf{r}(\mathbf{u};\epsilon) \,/\, \partial\epsilon^2$ and ρ is a positive constant. If the latter is interpreted as a referential mass density, and if the artificial viscosity c vanishes, then (135) furnishes an appropriate dynamical extension of the equilibrium equation. A physical viscosity may be included in the constitutive equations for $T_{i\alpha}$, but this is of no consequence here as (135) is intended solely to expedite the computation of equilibria.

Using (133) and (135) in (115) and (117), we obtain

$$\frac{\partial}{\partial \epsilon}\{E[\mathbf{r}(\mathbf{u};\epsilon)] + K[\mathbf{v}(\mathbf{u};\epsilon)]\} = -c\int_{\Omega}|\mathbf{v}|^2 da - c^{-1}(\int_{\partial\Omega_f}|\mathbf{t}|^2 ds + \int_{\partial\Omega_f}|\mathbf{m}|^2 ds), \quad (136)$$

where

$$K[\mathbf{v}(\mathbf{u};\epsilon)] = \frac{1}{2}\int_{\Omega}\rho|\mathbf{v}|^2 da \quad (137)$$

is the kinetic energy of the surrogate dynamical system and **t, m** respectively are again defined by $(120)_{1,2}$. Thus the total mechanical energy $E + K$ decays on solution trajectories of the dynamical system. Numerical integration of (133) and (135) again yields a minimizing sequence $\mathbf{r}_n(\mathbf{u}) = \mathbf{r}(\mathbf{u}; \epsilon_n)$, whose limit minimizes E.

To implement this method, we discretize (135) and the edge conditions (133) in space using an adaptation of a finite-difference mesh based on a discrete version of the Green-Stokes theorem with hour-glass control (Silling, 1988; Last and Harkness, 1989); and in ϵ - time using conditionally stable explicit central differences with zero initial velocity and initial positions with randomly distributed out-of-plane displacements. Finite difference methods based on a contour integral technique, such as what we use here, utilize approximations similar to those of four-node quadrilateral finite elements with reduced integration (Belytschko et al., 1982). Stable simulations are achieved by adjusting the artificial mass density and viscosity and repeating the computations, as needed, using successively smaller time steps, until the (non-dimensionalized) norms of the right-hand sides of (133) and (135) fall below a specified tolerance. A related procedure involving *kinetic damping* (Rezaiee-pajand et al., 2011) in lieu of viscous damping was used in Taylor et al. (2014) to simulate the nonlinear response of isotropic plates. The present problem is identical with respect to the implementation of the foregoing algorithm and, accordingly, we refer the interested reader to Section 3 of that work for a detailed exposition of the numerical solution scheme.

6. Numerical examples and discussion

We close with descriptions of a number of examples that highlight the effects of anisotropy on predicted deformations and wrinkle patterns. All simulations pertaining to transverse isotropy were conducted using the moduli $\beta = 5\ kPa$, $\mu_L = 1\ kPa$ and $\mu_T = 0.5\ kPa$ based on the study of fibrin gel by Namani et al. (2012). Those pertaining to orthotropy are based on the moduli (in units of *kPa*) $\mu = 1$, $\mu_a = 2$, $\mu_b = 1$, $\beta_a = 10$, $\beta_b = 5$ and $\beta_{ab} = 2.5$, chosen to be on the order of the fibrin gel but with one fiber orientation stiffer than the other. In the case of laminates, we take the laminae to be transversely isotropic with $\beta_{\pm} = 5$, $\mu_{L\pm} = 1$, and $\mu_{T\pm} = 0.5$ (in *kPa*), i.e. two layers of the fibrin gel material. These moduli satisfy inequalities (92) or (94), as appropriate. Figures 1–3 depict the deformed configurations of initially rectangular thin sheets having dimensions $10cm \times 25cm$ with a total thickness of $0.01cm$. Converged solutions were obtained using a regular 200×500 mesh. The vertical sides are free and the top and bottom edges are clamped at a relative separation of 1.2 times the initial value. The arrows in the figures indicate the orientations of the fibers on the reference plane and the vertical color scales show the distribution of out-of-plane displacement associated

with the wrinkling patterns. The crests of the wrinkles are oriented vertically in the case of isotropy (Taylor et al., 2014; Wang et al., 2019), whereas our simulations reveal a deviation from verticality due either to asymmetry in fiber orientation, to differing moduli for the two fiber families in the case of orthotropy, or to lamination with fibers oriented differently in laminae of various thicknesses. We see that the wrinkles orient themselves towards the direction of strongest fiber reinforcement. In In Figure 3, and subsequent figures involving transverse isotropy, a light arrow indicates the fiber direction in the thinner lamina and the heavier arrow the fiber direction in the thicker lamina.

Figures 4–6 show the deformed configurations of a very thin initially square sheet of side $50\,cm$ and thickness $0.0001\,cm$ in which the corners are displaced diagonally by different asymmetric amounts, indicated in the figure captions. This example is inspired by experiments conducted by Wong and Pellegrino (2006), albeit on isotropic sheets. All sides are free except for short vertical and horizontal segments of length $1.5\,cm$, adjoining the corners, where the sheet is clamped. The upper panel of Figure 4 (a–c) illustrates the significant effect of fiber orientation on the predicted deformation pattern at fixed diagonal displacement; the lower panel (d-f) illustrates the effect of varying diagonal displacements with a given fiber orientation. With a fiber orientation of 45°, the sheets display wrinkle patterns akin to those found by Wong and Pellegrino (2006) in an isotropic polyimide film at various ratios of asymmetric corner stretch. However, the patterns corresponding to orientations of 0° and 90° are quite different. The effects of fiber orientation in orthotropic and laminated plates, with laminae of equal thickness, are illustrated in Figures 5 and 6, respectively. Converged simulations were achieved using a regular 300 × 300 mesh.

Figures 7–9 pertain to an initially rectangular $38\,cm \times 12.8\,cm$ sheet of thickness $0.0025\,cm$. The vertical edges are free and the horizontal edges clamped, with the top edge displaced to the right uniformly by $0.256\,cm$, and converged solutions were achieved using a regular 600 × 200 mesh. This example also has an experimental counterpart, described in Wong and Pellegrino (2006), and was simulated in the case of isotropy in Taylor et al. (2014). Figure 7 illustrates the strong effect of fiber orientation in the case of transverse isotropy, in both wrinkle magnitude and orientation, whereas Figures 8 and 9, respectively, indicate that the effect is less pronounced in the case of orthotropy or lamination when the laminae have equal thickness.

In Figures 10–12, we display an annular sheet subjected to azimuthal shear. The initial inner and outer diameters are $4\,cm$ and $10\,cm$ and the thickness is $0.005\,cm$. The circular boundaries are clamped with the outer boundary fixed at its initial configuration and the inner rotated counter-clockwise by 10°. Converged solutions were obtained using a polar mesh consisting of 60 radial nodes and 360 circumferential nodes biased logarithmically towards the central hub. Figure 10, pertaining to transverse isotropy, demonstrates the strong effect of fiber orientation. In the top panel the fibers are oriented horizontally or vertically. The deformation pattern exhibits reflection symmetry with respect to either axis, with one pattern corresponding, as expected, to a 90° rotation relative to the other. The bottom panel indicates that significant differences in the patterns of wrinkling occur in annuli with fibers oriented radially and azimuthally. These, however, exhibit rotational symmetry in the sense that the predicted pattern, though clearly varying with radius, does not vary with azimuth.

Figures 11a,b, pertaining to orthotropy, indicate that the deformation pattern reflects the four-fold symmetry of the underlying fiber orientation. Rotation of this orientation is seen to produce a corresponding rotation of the deformation pattern. The situation is naturally different in the case of fibers oriented radially and circumferentially (Fig. 11c), with the deformation pattern again exhibiting rotational symmetry in this case. Similar conclusions apply to laminated annuli consisting of equal-thickness laminae (Fig. 12).

Finally, Figures 13–15 depict the response of an initially rectangular $12.5cm \times 5cm$ sheet of thickness $0.001cm$ with a central circular hole of radius $1.5cm$. The vertical edges and the edge of the hole are free, while the horizontal edges are clamped and displaced to 1.10 times their initial separation distance. Converged solutions were obtained using a polar mesh with 100 radial nodes and 400 circumferential nodes. Figure 13 illustrates the symmetric deformation patterns produced when the fibers are oriented parallel to the initial edges of the sheet, whereas asymmetry is observed when the fibers are orientated at 45° to these axes. Wrinkling is widespread, and we observe small triangular floppy zones adjoining the hole boundary where the sheet is lightly stressed. Similar patterns may be observed in desk-top experiments on hand-held sheets of rubber. In Figure 14a we, observe a symmetric deformation pattern in the case of orthotropy with the fibers aligned initially with the edges of the sheet. A slight asymmetry is observed for fibers oriented at 45° and 135°, (Fig. 14b) due to differences in the moduli associated with the two fiber families. Figures 15a,c exhibit symmetric deformation patterns in laminates composed of laminae of equal thickness having the same material properties, with fibers either aligned with the edges of the rectangle or symmetrically disposed with respect to them. The effect of different laminae thicknesses is to produce a slight asymmetry in the deformation pattern, depicted in Figure 15b.

Acknowledgements

MT acknowledges the support of start-up funding from Santa Clara University's School of Engineering. YD and JG gratefully acknowledge support provided by the US NIH through grants R01-HL-077921, R01-HL-118627 and U01-HL-119578. MS and DJS gratefully acknowledge partial support provided by the US NSF through grant CMMI-1538228.

References

Aguiar AR, 2019 Strong ellipticity conditions for orthotropic bodies in finite plane strain. J. Elast 134, 219–234.

Atai A, Steigmann DJ, 2014 Numerical analysis of wrinkled, anisotropic, nonlinearly elastic membranes. Mech. Res. Comm 57, 1–5.

Ayoub S, Ferrari G, Gorman RC, Gorman JH, Schoen FJ, Sacks MS, 2016 Heart valve biomechanics and underlying mechanobiology. Compr. Physiol 6, 1743–1780. [PubMed: 27783858]

Ball JM, Currie JC, Oliver PJ, 1981 Null Lagrangians, weak continuity, and variational problems of arbitrary order. J. Funct. Anal 41, 135–174.

Belytschko TB, Liu WK, Kennedy JM, 1982 Hourglass control for linear and nonlinear problems In: Atluri S, Perrone N (Eds.), Recent Development in Computing Methods for Nonlinear Structural Mechanics. ASME, Houston.

Ciarlet PG, 2005 An introduction to differential geometry with applications to elasticity. J. Elasticity 78-79, 3–201.

Dacarogna B, 1989 Direct Methods in the Calculus of Variations. Springer, Berlin and Heidelberg.

Deng X, Pellegrino S, 2012 Wrinkling of orthotropic viscoelastic membranes. AIAA Journal 50 (3), 668–681.

Flügge W, 1972 Tensor Analysis and Continuum Mechanics. Springer, Berlin, Heidelberg, and New York.

Fosdick RL, MacSithigh GP, 1986 Minimization in incompressible nonlinear elasticity theory. J. Elast 16, 267–301.

Fu C, Wang T, Xu F, Huo P, Potier-Ferry M, 2019 A modeling and resolution framework for wrinkling in hyperelastic sheets at finite membrane strain. J. Mech. Phys. Solids 124, 446–470.

Gerngross T, Pellegrino S, 2009 Anisotropic viscoelasticity and wrinkling of superpressure balloons: simulation and experimental verification In: AIAA Balloon Systems Coference. AIAA-2009-2633, Palm Springs, CA.

Grashow JS, Sacks MS, Liao J, Yoganathan AP, 2006a Planar biaxial creep and stress relaxation of the mitral valve anterior leaflet. Ann. Biomed. Eng 34, 1509–1518. [PubMed: 17016761]

Grashow JS, Yoganathan AP, Sacks MS, 2006b Biaxial stress-stretch behavior of the mitral valve anterior leaflet at physiologic strain rates. Ann. Biomed. Eng 34, 315–325. [PubMed: 16450193]

Healey TJ, Li Q, Cheng RB, 2013 Wrinkling behavior of highly stretched rectangular elastic films via parametric global bifurcation. J. Nonlin. Sci 23, 777–805.

Koiter WT, 1960 A consistent first approximation in the general theory of thin elastic shells. In: Koiter WT (Ed.), Proc: IUTAM Sumposium on the Theory of Thin Elastic Shells Delft, North-Holland, Amsterdam.

Koiter WT, 1966 On the nonlinear theory of thin elastic shells. Proc: Knonklijke Nederlandse Akademie van Wetenschappen 869, 1–54.

Last NC, Harkness RM, 1989 Kinematic (or hour-glass) mode control for a uniform strain quadrilateral by an assumed strain technique. Int. J. Num. Anal. Mech. in Geomechanics 13, 381–410.

Le Dret H, Raoult A, 1996 The membrane shell model in nonlinear elasticity: A variational asymptotic derivation. J. Nonlin. Sci 6, 59–84.

Merodio J, Ogden RW, 2003 A note on strong ellipticity for transversely isotropic linearly elastic solids. Q. J. Mech. Appl. Math 56, 589–591.

Namani R, Feng Y, Okamoto RJ, Jesurai N, Sakiyama-Elbert SE, Genin GM, Bayy PV, 2012 Elastic characterization of transversely isotropic soft materials by dynamic shear and asymmetric indentation. J. Biomech. Engng 134, 061004-1–061004-11. [PubMed: 22757501]

Nayyar V, Ravi-Chandar K, Huang R, 2011 Stretch-induced stress pattern and wrinkles in hyperelastic thin sheets. Int. J. Sol. Struct 48, 3471–3483.

Payton RG, 1983 Elastic Wave Propagation in Transversely Isotropic Media. Martinus Nijhoff, The Hague.

Pipkin AC, 1994 Relaxed energy densities for large deformations of membranes. IMA J. Appl. Math 52, 297–308.

Puntel E, Deseri L, Fried E, 2011 Wrinkling of a stretched thin sheet. J. Elasticity 105, 137–170.

Qin Z, Taylor M, Hwang M, Bertoldi K, Buehler MJ, 2014 Effect of wrinkles on the surface area of graphene: Toward the design of nanoelectronics. Nano Lett 14 (11), 6520–6525. [PubMed: 25299933]

Rezaiee-pajand M, Kadkhodayan M, Alamatian J, Zhang L, 2011 A new method of fictitious viscous damping determination for the dynamic relaxation method. Comp. Struct 89, 783–794.

Sacks MS, Yoganathan AP, 2007 Heart valve function: a biomechanical perspective. Philos. Trans. R. Soc. Lond B362, 1369–1391.

Shirani M, Steigmann DJ, 2019 Asymptotic derivation of nonlinear plate models from three-dimensional elasticity theory In: Altenbach H, Chroscielewski J, Eremeyev V (Eds.), Recent Developments in the Theory of Shells. Springer (in press).

Shugar T, 1990 Automated dynamic relaxation solution algorithms for compliant systems. Tech. Rep. N-1812, Naval Civil Engineering Laboratory, Port Hueneme, CA.

Silling SA, 1988 Finite difference modeling of phase changes and localization in elasticity. Comp. Meth. Appl. Mech. Eng 70, 251–273.

Sipos AA, Fehér E., 2016 Disappearance of stretch-induced wrinkles of thin sheets: A study of orthotropic films. Int. J. Solids Struct 97-98, 275–283.

Spencer AJM, 1984 Constitutive theory for strongly anisotropic solids In: Spencer AJM (Ed.), Continuum Theory of the Mechanics of Fibre-Reinforced Composites. Vol. 282 Springer, Vienna and New York, pp. 1–32, cISM Courses and Lectures.

Steigmann DJ, 1986 Proof of a conjecture in elastic membrane theory. ASME J. Appl. Mech 53, 955–956.

Steigmann DJ, 2010 Applications of polyconvexity and strong ellipticity to nonlinear elasticity and elastic plate theory In: Schröder J, Neff P (Eds.), Applications of Poly-, Quasi-, and Rank-One Convexity in Applied Mechanics. Vol. 516 Springer, Vienna and New York, pp. 265–299, cISM Courses and Lectures.

Steigmann DJ, 2012 Refined theory for linearly elastic plates: laminae and laminates. Math. Mech. Solids 17, 351–363, corrigendum: MMS 17 (2012), 666.

Steigmann DJ, 2017 Finite Elasticity Theory. Oxford University Press.

Steigmann DJ, 2018 Equilibrium of elastic lattice shells. J. Engng. Math 109, 47–61.

Taylor M, Bertoldi K, Steigmann DJ, 2014 Spatial resolution of wrinkle patterns in thin elastic sheets at finite strain. J. Mech. Phys. Solids 62, 163–180.

Taylor M, Davidovitch B, Qiu Z, Bertoldi K, 2015 A comparative analysis of numerical approaches to the mechanics of elastic sheets. J. Mech. Phys. Solids 79, 92–107.

Topping BHV, Khan AI, 1994 Parallel computation schemes for dynamic relaxation. Eng. Comp 11 (6), 513–548.

Toupin RA, 1962 Elastic materials with couple-stresses. Arch. Rational Mech. Anal 11, 385–414.

Toupin RA, 1964 Theories of elasticity with couple-stress. Arch. Rational Mech. Anal 17, 85–112.

Wang T, Fu C, Xu F, Huo Y, Potier-Ferry M, 2019 On the wrinkling and restabilization of highly stretched sheets. Int. J. Engng. Sci 136, 1–16.

Wenk JF, Ratcliffe MB, Guccione JM, 2012 Finite element modeling of mitral leaflet tissue using a layered shell approximation. Med. Biol. Eng. Comput 50, 1071–1079. [PubMed: 22971896]

Wong YW, Pellegrino S, 2006 Wrinkled membranes part i: experiments. J. Mech. Mat. Struct 1, 3–25.

Woo K, Igawa H, h. Jenkins C, 2004 Analysis of wrinkling behavior of anisotropic membrane. CMES 6 (4), 397–408.

Zhang W, Ayoub S, Liao J, Sacks MS, 2016 A meso-scale layer-specific structural constitutive model of the mitral heartvalve leaflets. Acta Biomater 32, 238–255. [PubMed: 26712602]

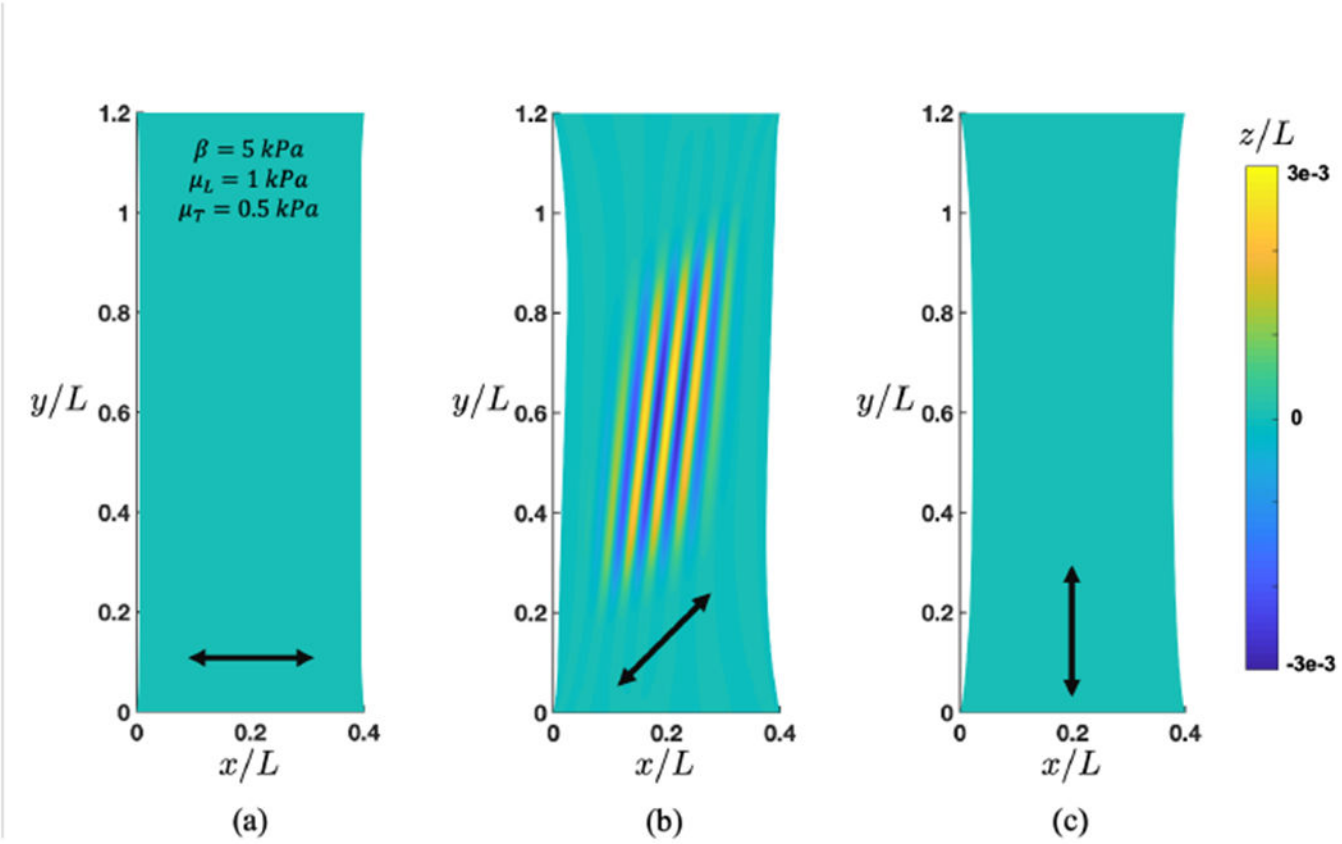

Figure 1:

Axial stretch of a fibrin gel sheet reinforced with a single family of fibers oriented at (a) 0°, (b) 45°, and (c) 90° to the horizontal axis. Non-dimensionalized by sheet height ($L = 25cm$)

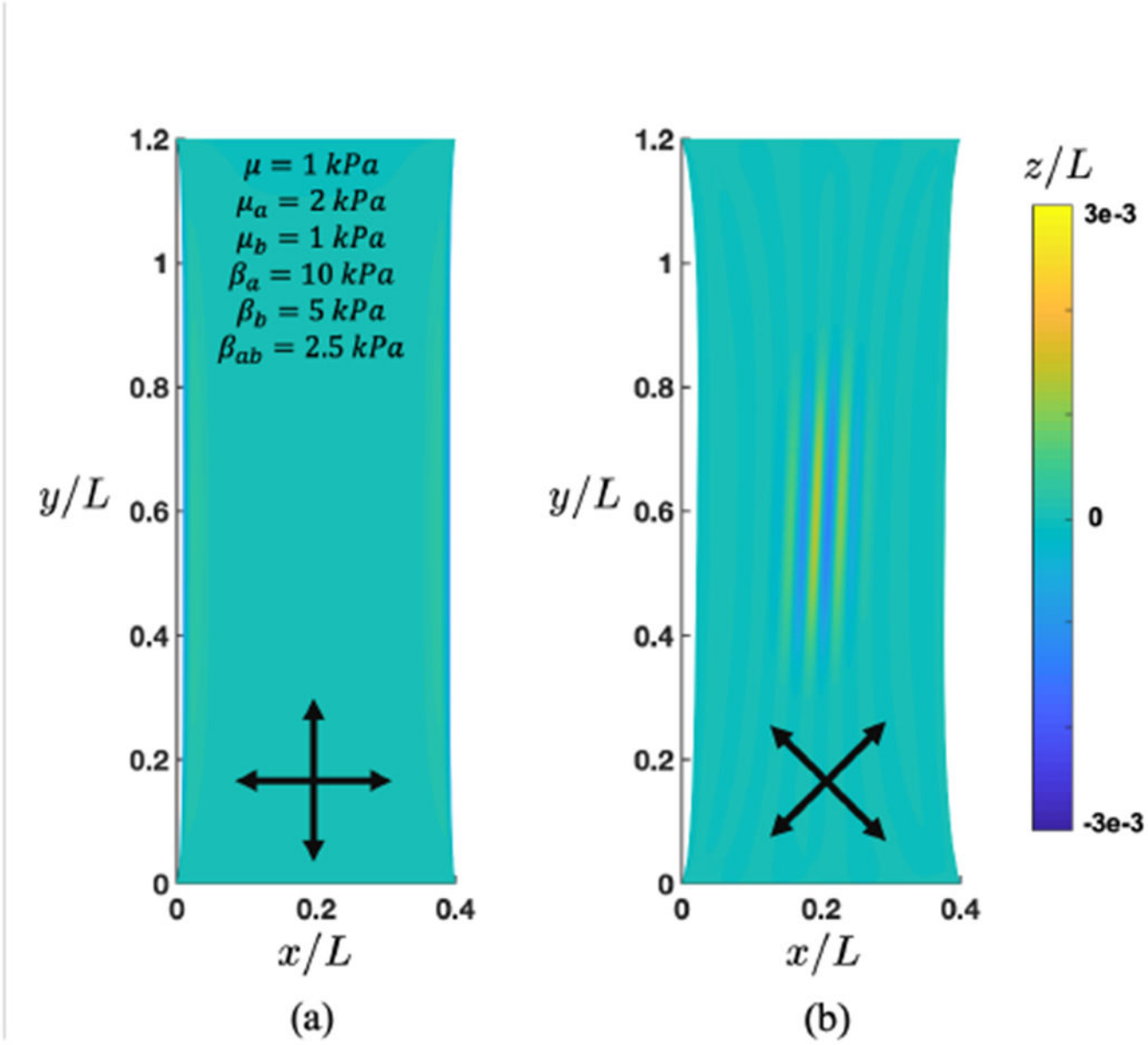

Figure 2:
Axial stretch of an orthotropic gel sheet reinforced with two families of fibers oriented at (a) 0°/90° and (b) 45°/135°. Non-dimensionalized by sheet height ($L = 25cm$)

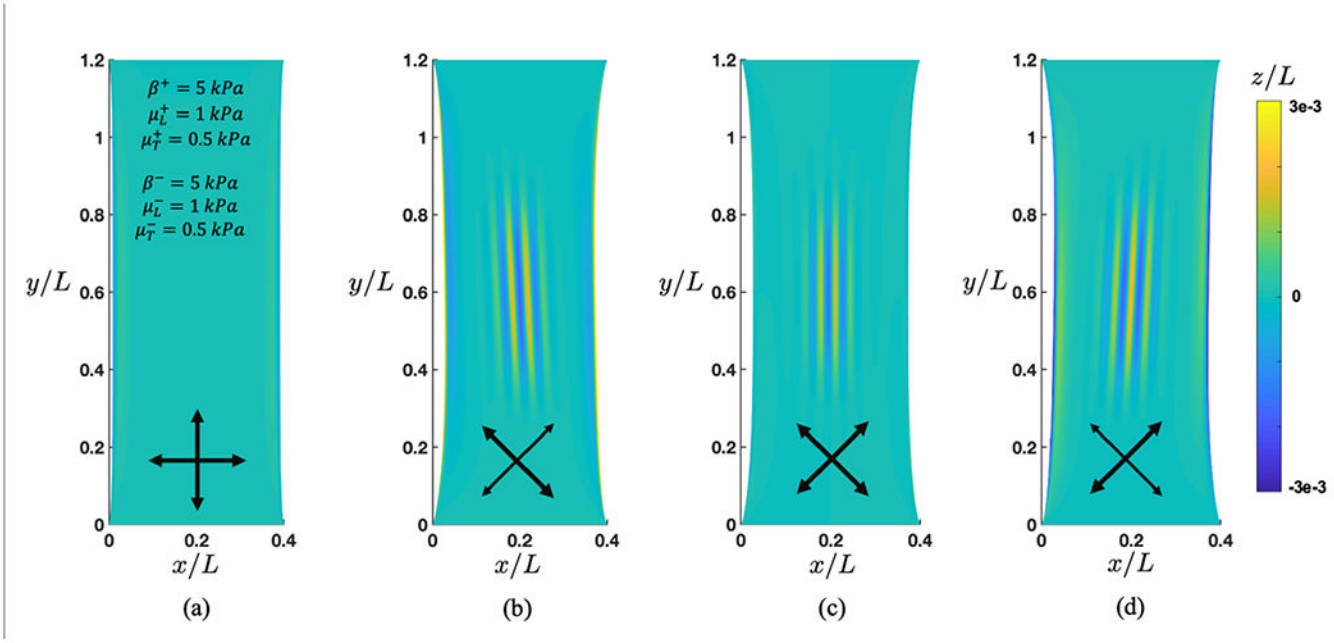

Figure 3:

Axial stretch of a two-layer fibrin gel laminate with upper/lower surface fiber orientations of (a) 0°/90° ($\eta = 0.5$), (b) 45°/135° ($\eta = 0.25$), (c) 45°/135° ($\eta = 0.5$), and (d) 45°/135° ($\eta = 0.75$). Non-dimensionalized by sheet height ($L = 25cm$)

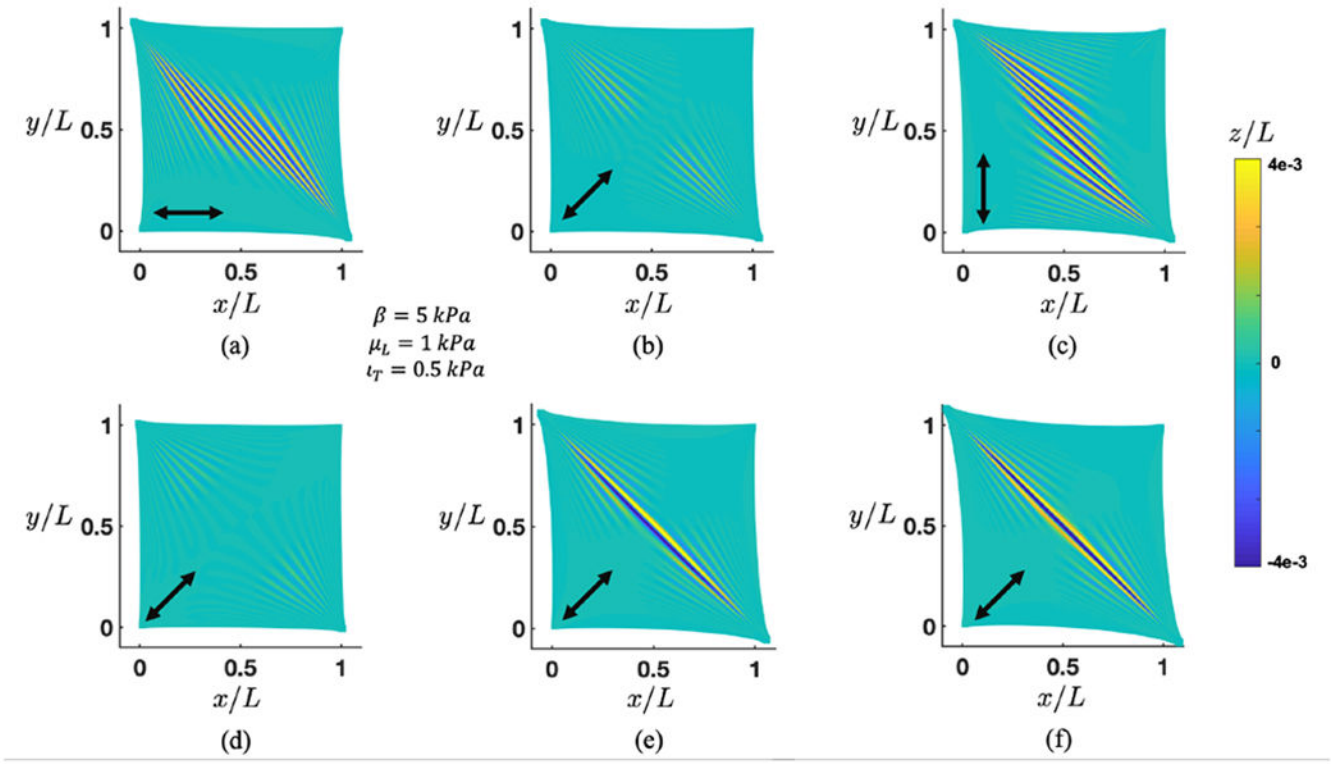

Figure 4:

Square transversely isotropic fibrin gel sheet with asymmetric tensile corner displacements. Upper right and bottom left corner stretched diagonally by a factor of 1.01. (a-c) Opposing corners stretched by a factor of 1.1 with fiber orientations of 0°, 45°, and 90°, respectively. (d-f) Fiber orientation fixed at 45° but with opposing corners stretched by factors of 1.05, 1.15, and 1.2, respectively. Non-dimensionalized by sheet height ($L = 50 cm$)

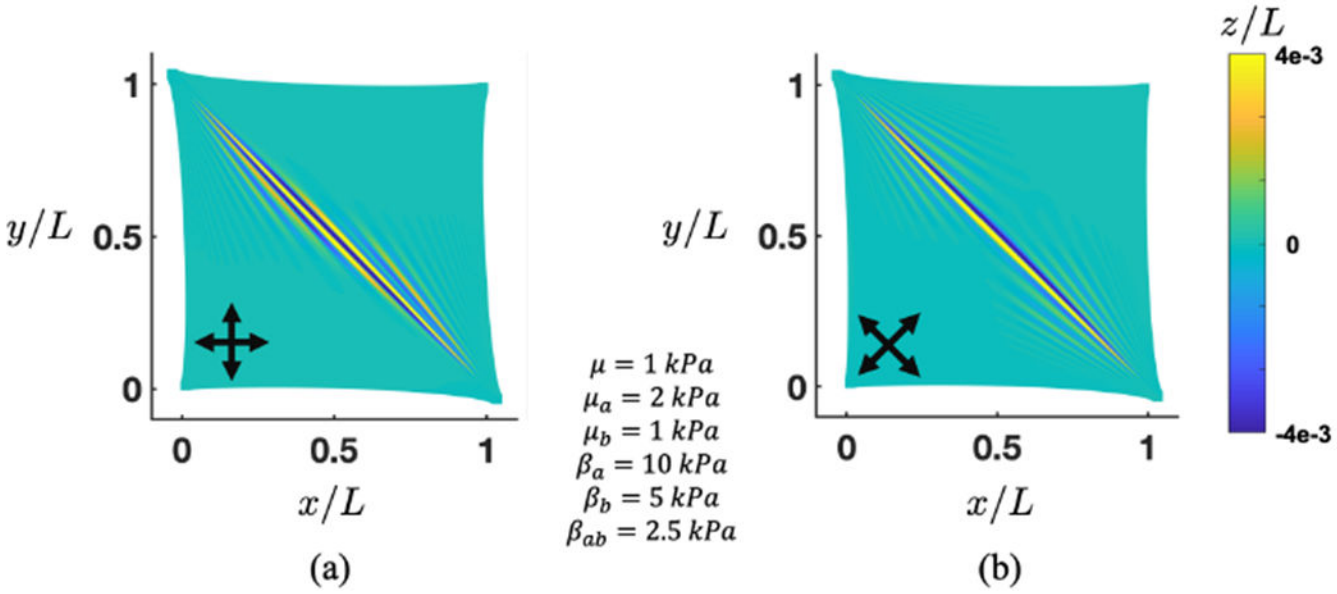

Figure 5:

Square orthotropic gel sheet with asymmetric tensile corner displacements. Upper right and bottom left corner stretched diagonally by a factor of 1.01; opposite corners stretched by a factor of 1.1. (a) Fiber families oriented at 0° and 90°. (b) Fiber families oriented at 45° and 135°. Non-dimensionalized by sheet height ($L = 50 cm$)

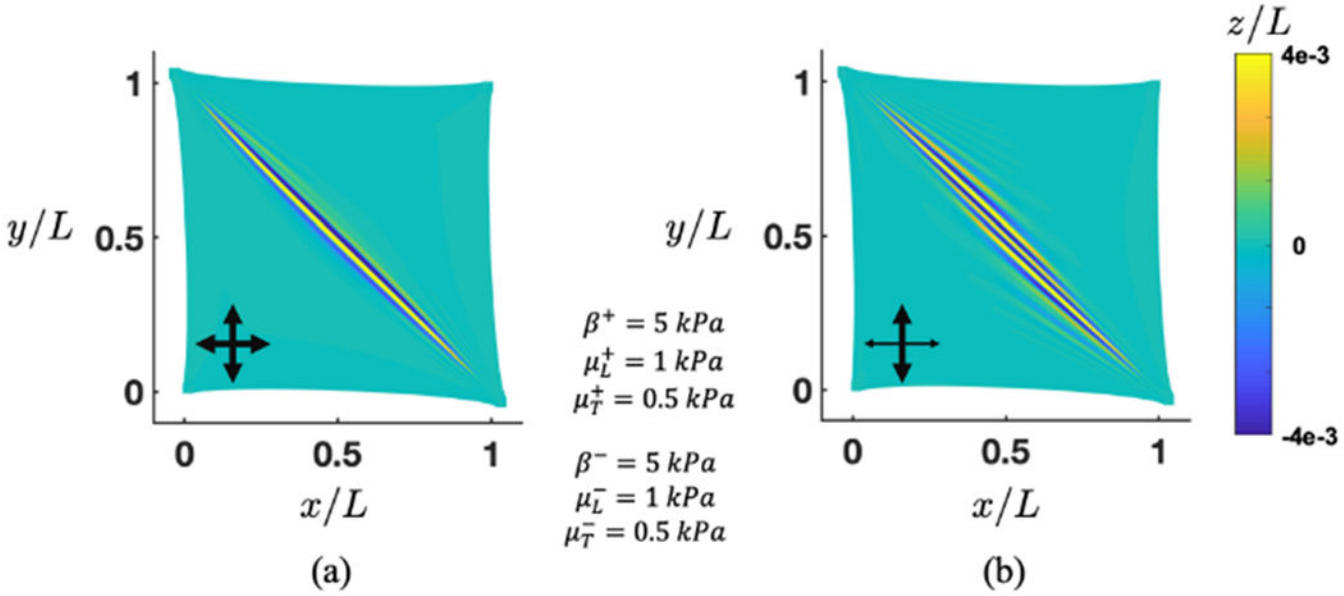

Figure 6:

Square two-layer fibrin gel laminate with asymmetric tensile corner displacements. Upper right and bottom left corner stretched diagonally by a factor of 1.01; opposite corners stretched by a factor of 1.1. Fiber families oriented at 0° (upper layer) and 90° (lower layer) with (a) $\eta = 0.5$ and (b) $\eta = 0.25$. Non-dimensionalized by sheet height ($L = 50 cm$)

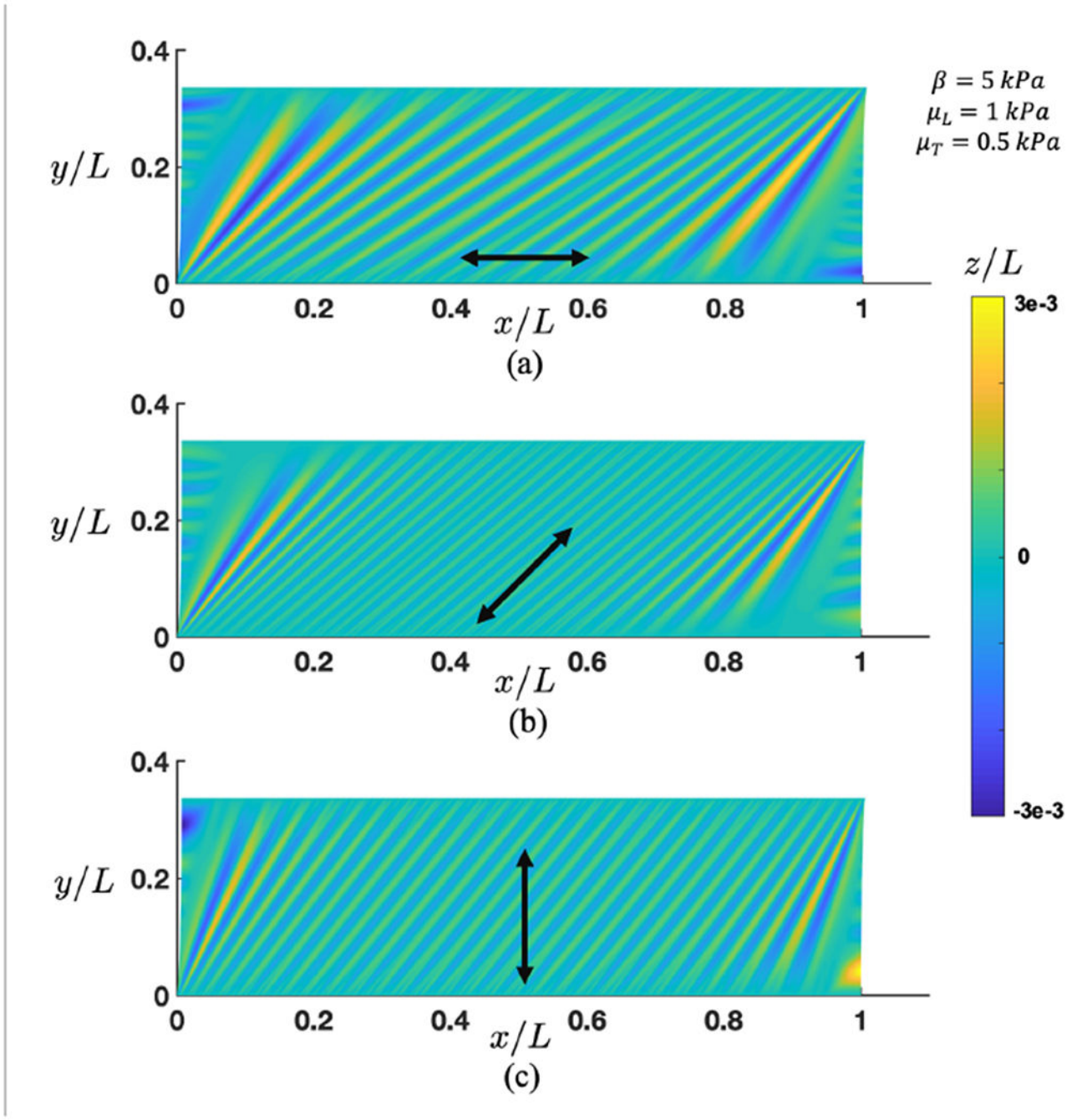

Figure 7:
Fibrin gel sheet in shear for fiber families of (a) 0°, (b) 45°, and (c) 90°. Non-dimensionalized by sheet width ($L = 38 cm$)

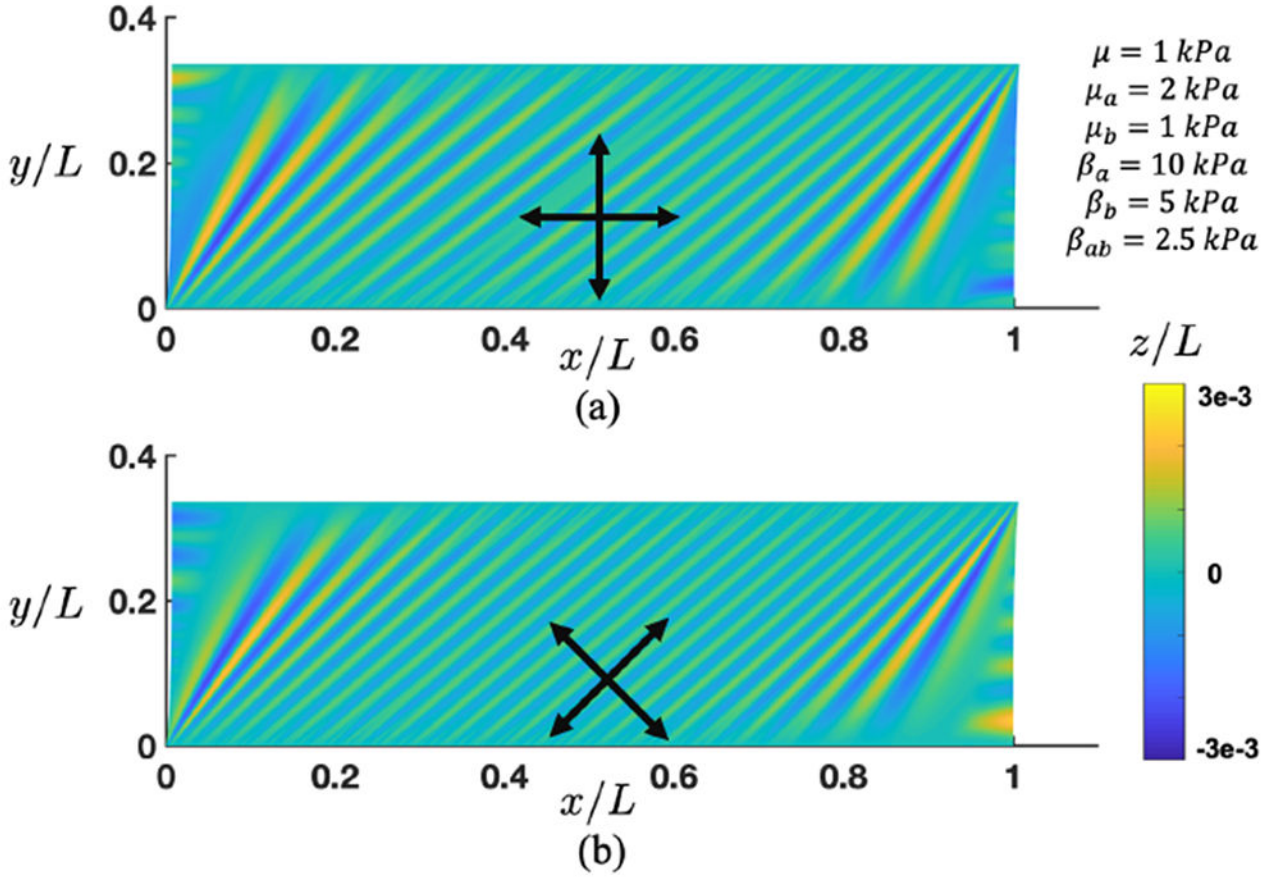

Figure 8:

Shearing of orthotropic gel sheet with fibers families of (a) 0° /90° and (b) 45°/135°. Non-dimensionalized by sheet width ($L = 38 cm$)

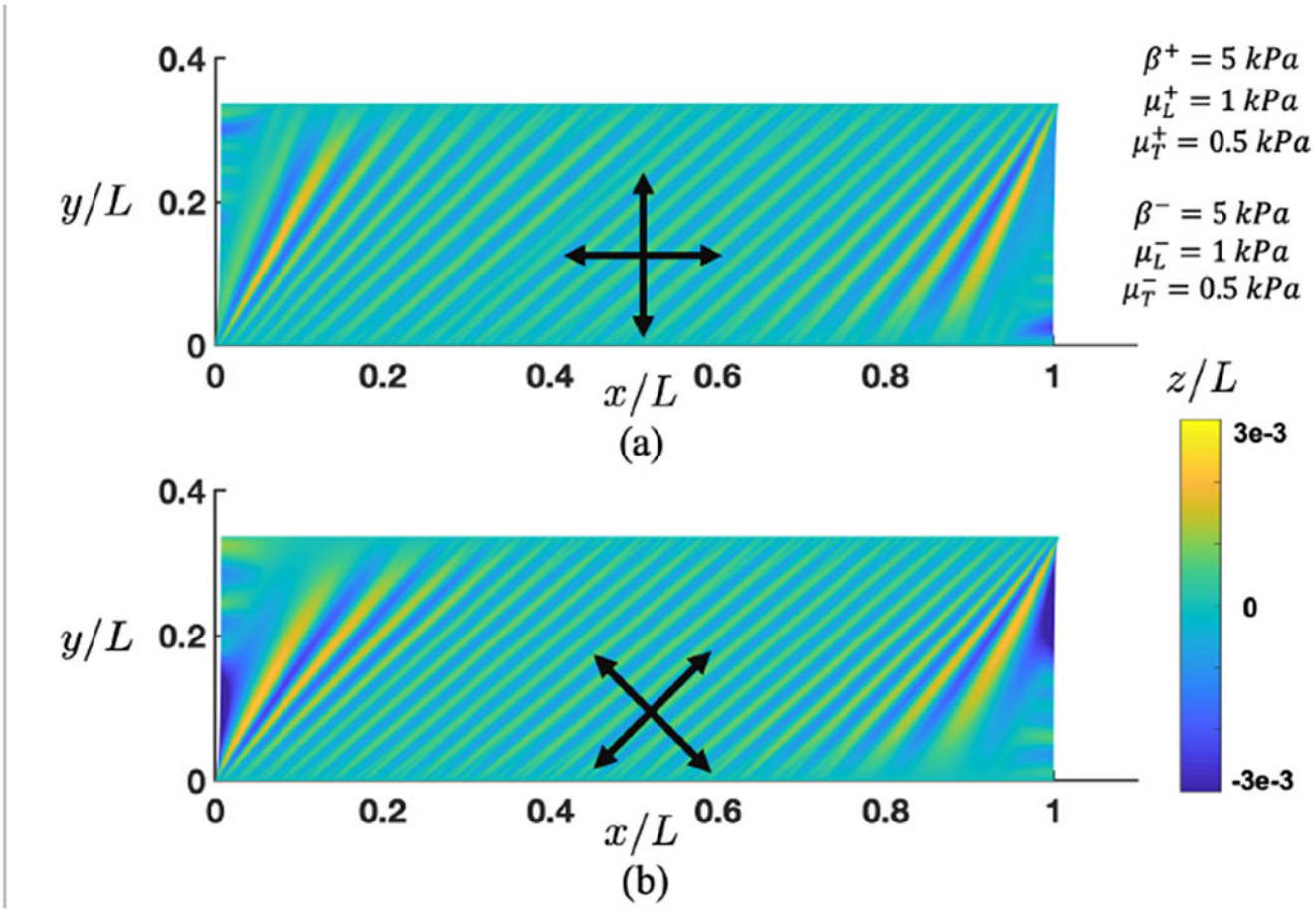

Figure 9:
Shearing of a two-layer fibrin gel laminate with fiber families of (a) 0° (upper layer) & 90° (lower layer) and (b) 45° (upper layer) & 135° (lower layer). Non-dimensionalized by sheet width ($L = 38cm$)

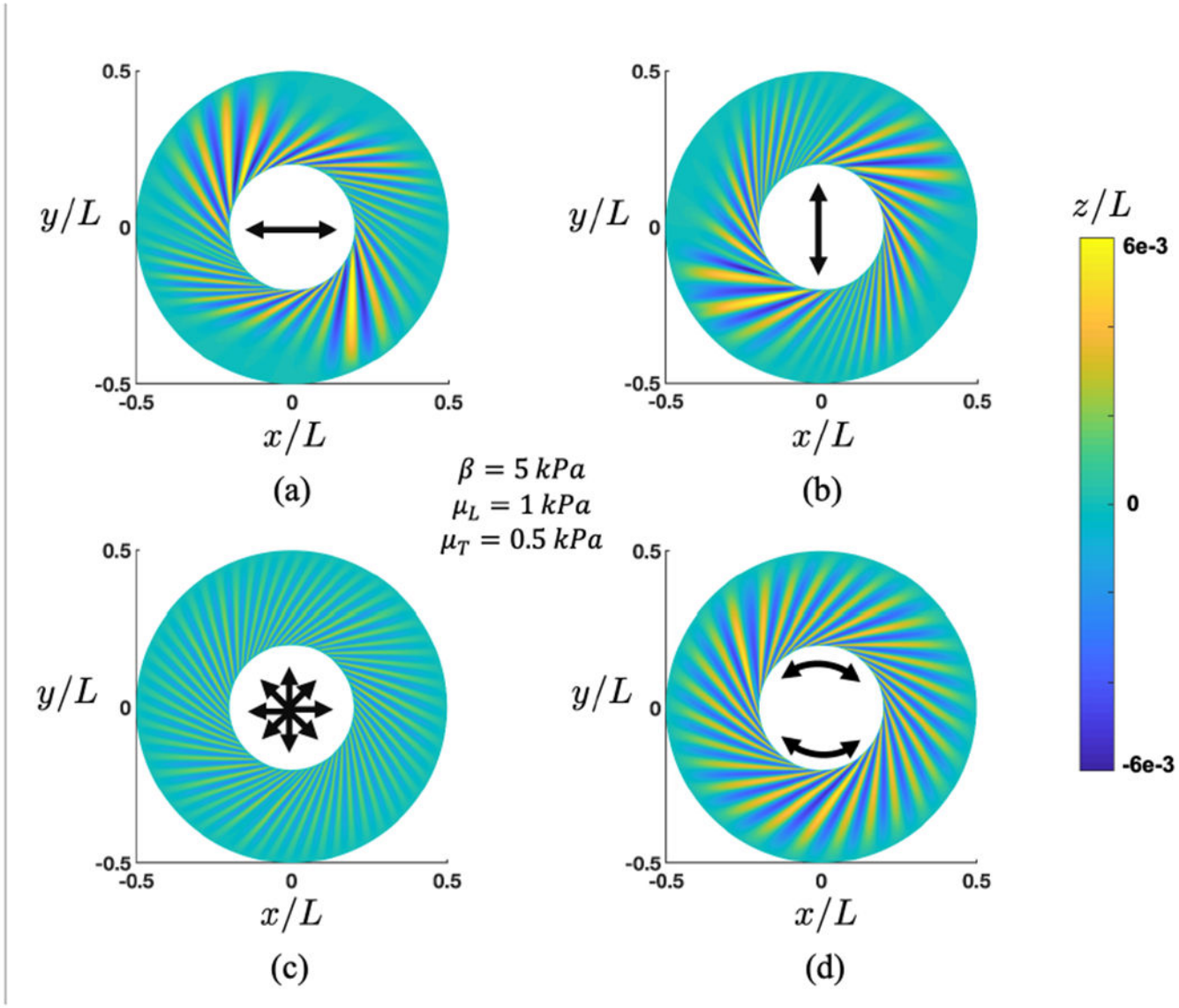

Figure 10:

Annular fibrin gel sheet with inner hub twisted 10° counter-clockwise for fiber families oriented (a) at 0°, (b) at 90°, (c) radially, and (d) circumferentially. Non-dimensionalized by outer diameter ($L = 10cm$)

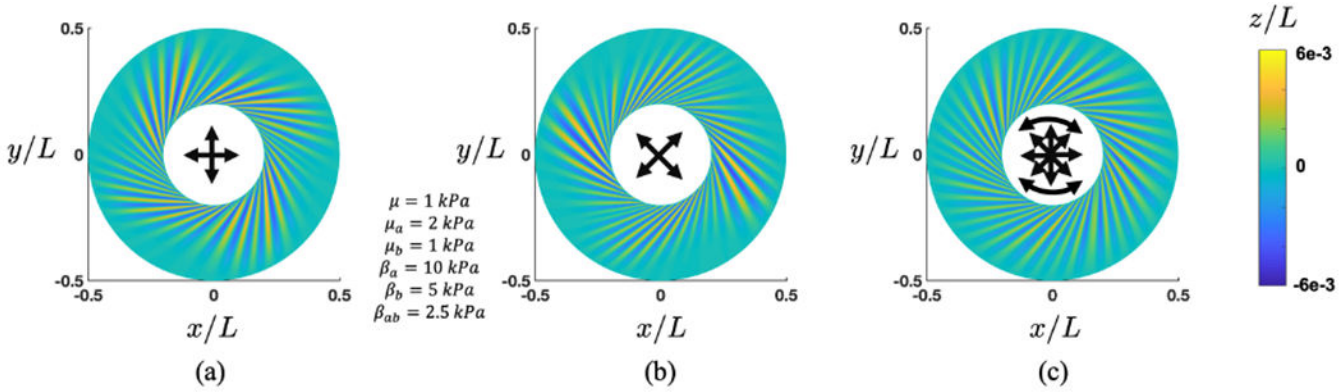

Figure 11:

Annular orthotropic gel sheet with inner hub twisted 10° counter-clockwise for fiber families oriented (a) at 0°/90°, (b) at 45°/135°, and (c) radially/circumferentially. Non-dimensionalized by outer diameter ($L = 10 cm$)

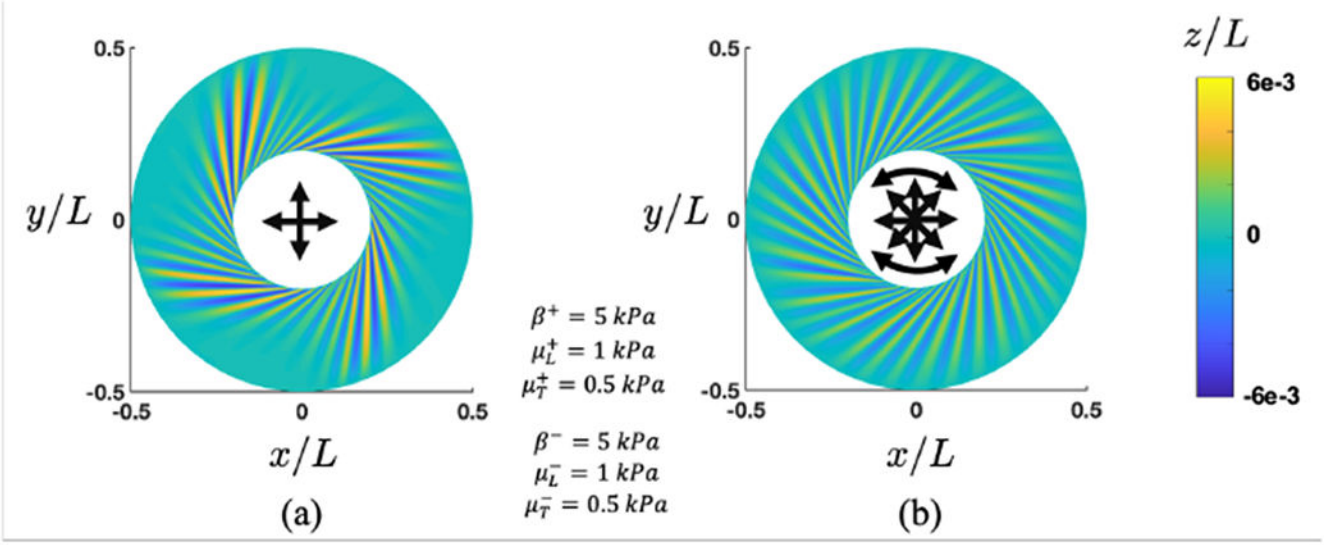

Figure 12:

Annular two-layer fibrin gel laminate with inner hub twisted 10° counter-clockwise for fiber families oriented (a) at 0°/90° and (b) radially/circumferentially. Non-dimensionalized by outer diameter ($L = 10cm$)

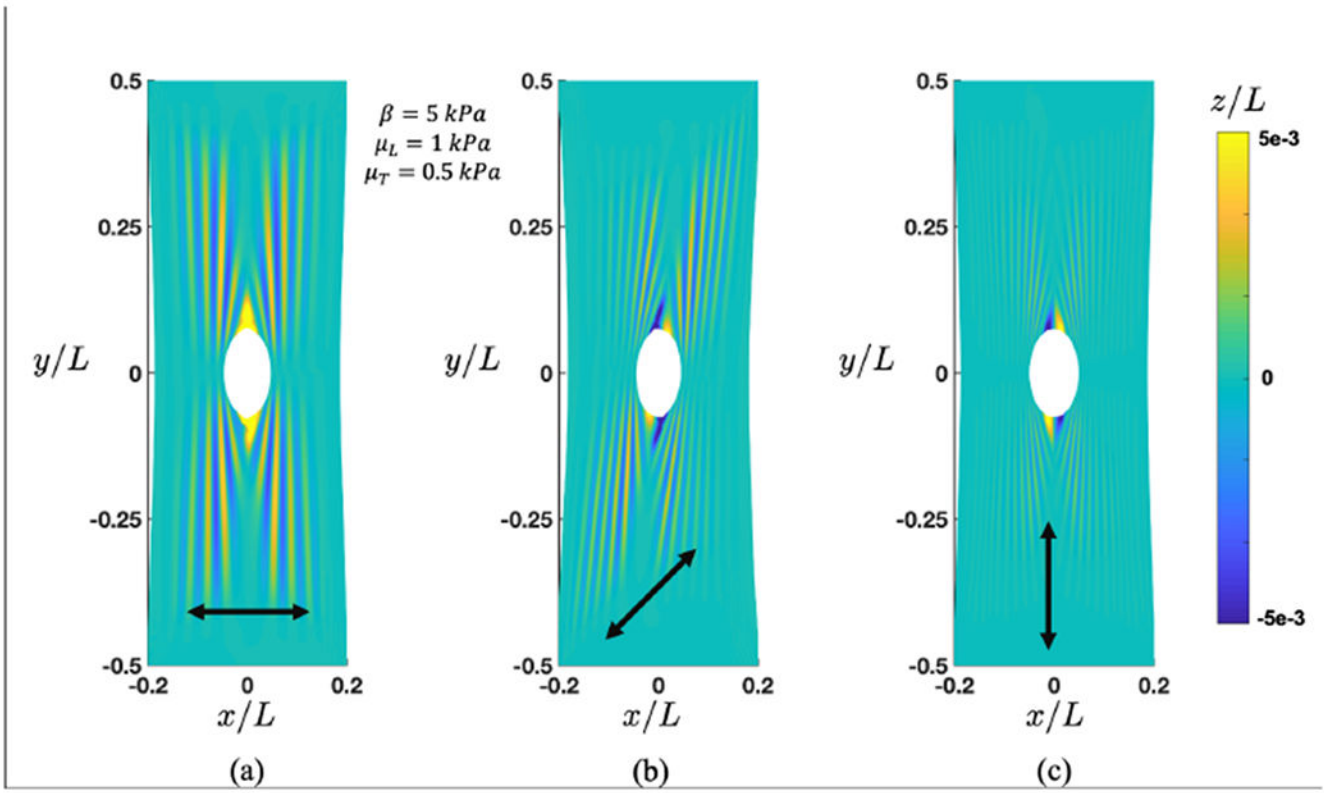

Figure 13:

Axial stretch of a fibrin gel sheet with traction-free central hole reinforced with a single family of fibers oriented at (a) 0°, (b) 45°, and (c) 90° to the horizontal axis. Non-dimensionalized by sheet height (L = 12.5cm)

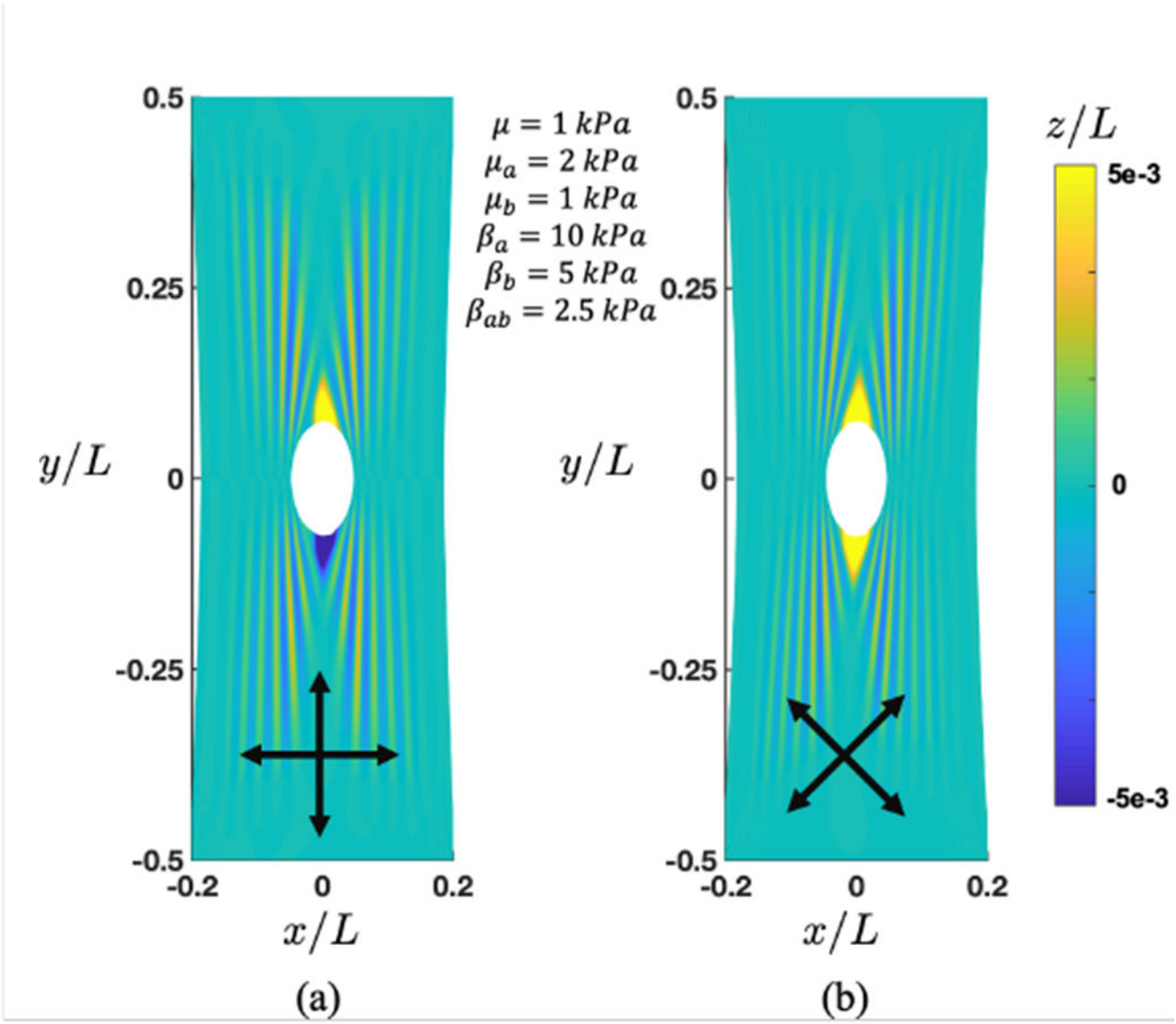

Figure 14:
Axial stretch of an orthotropic gel sheet with traction-free central hole reinforced with two families of fibers oriented at (a) 0°/90° and (b) 45°/135°. Non-dimensionalized by sheet height ($L = 12.5cm$)

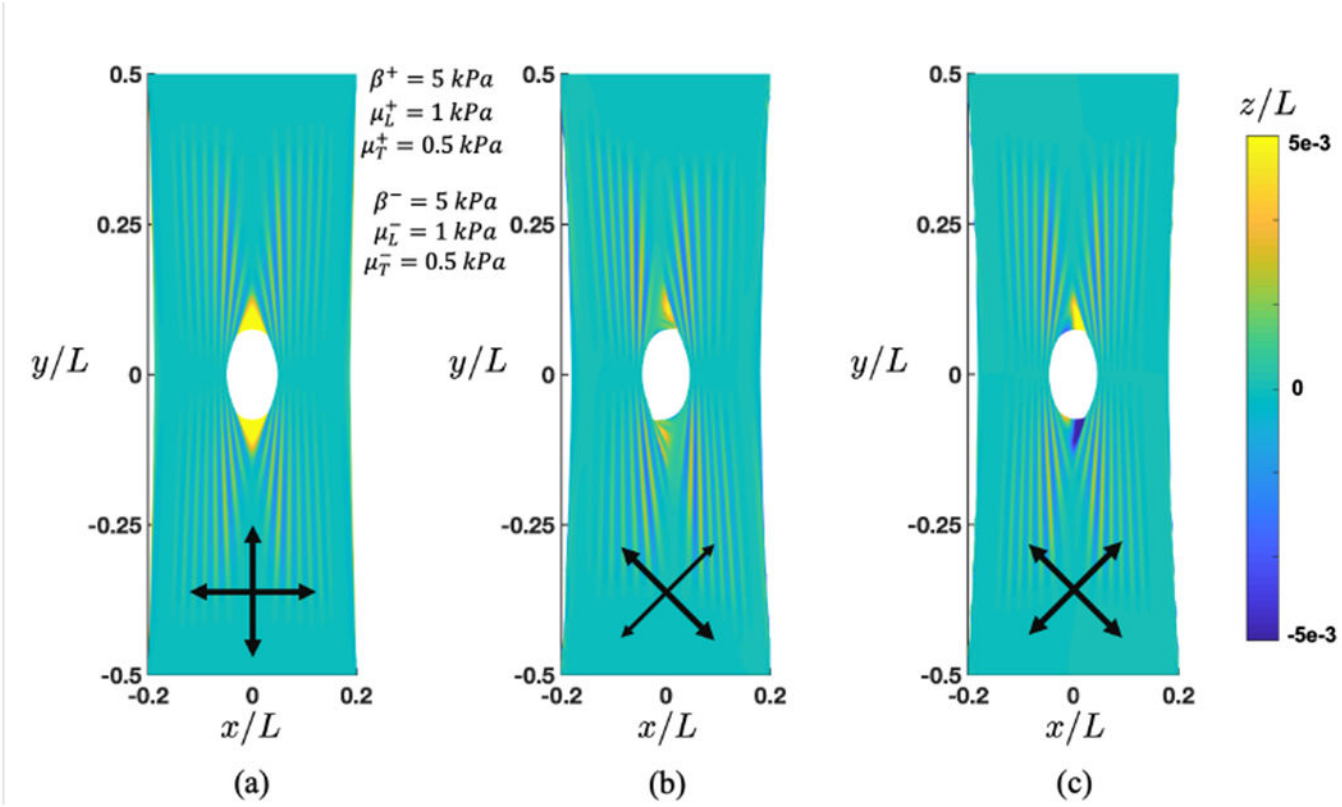

Figure 15:

Axial stretch of a two-layer fibrin gel laminate with traction-free central hole with upper/lower surface fiber orientations of (a) 0°/90° ($\eta = 0.5$), (b) 45°/135° ($\eta = 0.25$), and (c) 45°/135° ($\eta = 0.5$). Non-dimensionalized by sheet height ($L = 12.5cm$)